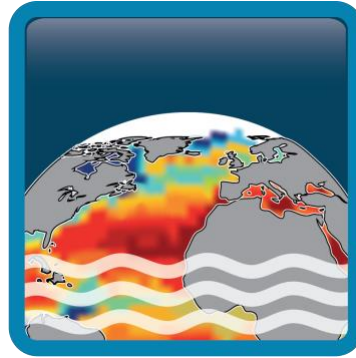


Climate Change Initiative+ (CCI+) Phase 1

Sea Surface Salinity



Product Validation and Intercomparison Report (PVIR)

Customer: ESA

Ref.: ESA-CCI-PRGM-EOPS-SW-17-0032

Version: v3.0

Ref. internal: AO/1-9041/17/I-NB_v1r2


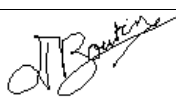

Revision Date: 12/09/2021

Filename: SSS_cci-D4.1-PVIR-v3.0.docx

Deliverable code: D4.1



Signatures

	Name	Signature	Date
Lead Author	Adrien Martin (NOC)		
Authors	S. Guimbard (OceanScope)		
	J. Koehler (University of Hamburg)		
	V.P. Akhil (CSIR-NIO), J. Vialard (LOCEAN)		
	O. Houdegnonto, N. Kolodziejczyk, N. Reul (Ifremer)		
Approved By	Jacqueline Boutin (Science Leader) LOCEAN		
	Nicolas Reul (Science Leader) IFREMER		
	Rafael Catany (Project Manager) ARGANS		
Accepted By	Susanne Mecklenburg (Technical Officer) ESA		

Diffusion List
Sea Surface Salinity Team Members
ESA (Susanne Mecklenburg, Roberto Sabia, Paolo Cipollini)

Amendment Record Sheet

	Document Change Record	
Date / Issue	Description	Section / Page
15-Oct-2019/v1r1	Template	Whole document
24-Dec-2019/v1r2	Final draft distributed to the team involved in validation	Whole document
10-Jan-2020/v1.0	Final Distribution to ESA	
7-Apr-2020/v1.1	The document has been updated using ISAS at 5 m depth, using only data with PCTVAR<95%. Comparison between ISAS and CCI has been proceeded on CCI grid not to affect CCI uncertainty estimate.	Section 4 / 27-54
	Old section 5.4.1 about comparison between CCI and CMEMS in river plume has been removed from the PVIR and included in the CAR.	Section 5.4.1 / p 71
	section 5.5 about case study 5: comparing salinity variability between observations and models has been added to the document (originaly was in the CAR)	Section 5.5 / p.74
	Four figures from Pi-MEP match-up mooring report representing SSS power spectra have been included in Annex C.	Annex C / p.115
	Update of the executive summary	Section 2 / p. 19-21
	A sentence to summarize what specific improvements of SMOS in the Bay of Bengual has been added.	Section 5.3 / p. 64
	The document has been reviewed for spelling/grammar/typos errors	Whole document
2-Nov-2020/v2.0	Version 2 final draft distributed to the team with the main new features: Update with CCI SSS version 2.3 data; Comparison between v1.8 and v2.3; Comparison between L4 and L3C for v2.3; Contrary to v1, ISAS is not used anymore as reference.	Whole document
11-Nov-2020/v2.0	Final distribution to ESA	
25-May-2021/v2.1	Minor corrections after ESA feedback	Whole document
September 2021/v3.0	Version 3 final draft distributed to the team with update using CCI SSS v3.2 instead of v2.3. It follows the same structure than PVIR v2 + outputs from the case studies	Whole document

Table of Contents

Signatures	iii
Amendment Record Sheet	v
List of figures	viii
List of tables	xi
1 Introduction	12
1.1 Purpose and scope	12
1.2 Structure of the document	12
1.3 Applicable Documents.....	12
1.4 Reference Documents	13
1.5 Acronyms.....	14
2 Executive Summary	15
2.1 Sea Surface Salinity products	15
2.2 Main results	15
2.3 Main results from Pi-MEP match-up reports	16
2.4 Recommendations and caveats to use CCI+SSS dataset	17
3 Validation: Data & Methods.....	18
3.1 Dataset description.....	18
3.1.1 Argo match-ups database: Pi-MEP MDB	18
3.1.2 Reference dataset: gridded MDB.....	19
3.2 Uncertainty validation	20
3.3 Quality metrics	21
4 Validation of Products, Stability, Resolution and Product Uncertainty Estimates	23
4.1 Accuracy & Precision.....	23
4.1.1 Products validation for L4	23
4.1.2 Products validation differences for Aquarius, SMAP, SMOS L3 products	28
4.1.3 Validation in the Bay of Bengal (Case study 3: V.P. Akhil, J. Vialard)	32
4.1.4 Comparison in Congo Plume (Case Study 4: O. Houndegnonto, N. Kolodziejczyk, N. Reul)	34
4.2 Time series stability: intra-annual & long-term stability	38
4.3 In situ vertical representiveness error	44
4.4 Temporal & spatial effective resolution	46
4.4.1 SSS temporal variability at different time scale (Case Study 5: J. Köhler, M. Sena-Martins, D. Stammer)	46
4.4.2 Temporal resolution.....	47
4.4.3 Assessment of mesoscale features in Tropical Atlantic (Case Study 4: N. Kolodziejczyk, N. Reul)	49
4.5 Uncertainty	54
4.5.1 Normalised SSS	55
4.5.2 Compared SSS distribution	56

List of figures

- Figure 1: (top-left) L4 CCIv3 monthly SSS for the 15th of January 2015, (top-right) Argo floats upper salinity measurements from the Pi-MEP MDB for the month of the 15th of January 2015. (middle/bottom-left) temporal median/robust standard deviation of L4 CCIv3 SSS. (middle/bottom-right) temporal median/robust standard deviation of the gridded MDB SSS. Dashed lines indicates pixel with less than 30 points over the full time-series.----- 24
- Figure 2: Same as Figure 1 middle-right but centred around the poles. ----- 25
- Figure 3: Histogram of all pairwise gridded MDB (left) Argo SSS in grey and CCI L4 v3 SSS in green; (right) Gridded MDB of the CCI L4 v3 minus Argo difference, (blue line) normalized probability function (PDF) using computed mean and std, (orange curve) normalized PDF using computed median and robust std. ----- 25
- Figure 4 (left) Temporal median and (right) temporal robust standard deviation of gridded pairwise SSS differences between CCI and Argo. (on the left) A moving window of 2 pixels in longitude and latitude is applied to the median in order to highlight statistical significance (at 95%) which are indicated with dots. (on the right) Robust standard deviation calculated with less than 30 valid grid points in time are hatched. ----- 27
- Figure 5: (top-left) temporal median of the CCI L3C SMOS difference against CCI L4 v3; (top-right) same but for the temporal std of the difference; (bottom-left) temporal median of the CCI L3C SMOS difference between Ascending and Descending passes; (bottom-right) temporal median of CCI L3C Aquarius SSS for ascending passes. ----- 29
- Figure 6: Normalised PDF of all CCI/Argo pairwise gridded MDB v3 for (grey) Argo, (blue) Aquarius, (orange) SMAP and (green) SMOS. ----- 30
- Figure 7: (left) temporal median of; (right) temporal classic std of the gridded MDB of the pairwise difference between CCI L3 combined asc+desc products and Argo for (top row) Aquarius; (second row) SMAP; (last row) SMOS. A moving window of 4 pixels in longitude and latitude is applied to the median (on the left) in order to highlight statistical significance (at 95%) which are indicated with dots. Std calculated with less than 30 valid grid points in time are hatched (on the right). 32
- Figure 8: Spatial coverage of the CCI+SSS (a) v1 and (b) v3 products. The various boxes used for the comparison to in situ data of Figure 9 are marked.----- 33
- Figure 9: Correlation, root-mean square difference and bias of the CCI+SSS v1 (red) and v3 (green) products comparison to in situ data over the entire Bay of Bengal (BoB), and over the various regions indicated on Figure 8 (NBoB, WBoB, CBoB, ANDA). Only data points which are collocated with the two datasets have been considered, so that the two datasets are evaluated over the same sample.----- 34
- Figure 10: Scatter plot of TSG SSS measurements (a) and Argo/CTD data (b) with the CCI+SSS v2.31 products in the Gulf of Guinea (15°S-10°N/10°W-15°E) over the period 2010-2019. (c) distribution of the difference of co-located in situ/CCI+SSSv2 (in pss) as a function of the distance from the coast. ----- 36
- Figure 11: (1st panel): mean SSS of gridded MDB of pairwise Argo in red and L4 CCI measurements in orange, green and black for v1, v2 and v3; (2nd panel) Average of; (3rd panel) standard deviation of; the gridded MDB of the pairwise SSS difference between CCI and Argo. Solid lines represent

(2nd panel) the median (3rd panel) the robust standard deviation. Dashed lines represent (2nd panel) the mean (3rd panel) the standard deviation. The shading indicates the 95% confidence interval. 4th panel) number of valid gridded MDB values. ----- 38

Figure 12 (1st panel): SSS mean of gridded MDB of the pairwise CCI and Argo measurement; (2nd panel) Median of; (3rd panel) robust standard deviation of; the gridded MDB of the pairwise SSS difference between CCI and Argo. (4th panel) number of valid gridded MDB values. The colours of the curves correspond to the data indicated in the legend. ----- 39

Figure 13: Global latitude-time Hovmöller of the gridded MDB of the pairwise CCI difference with Argo for (top) L4 v3; (middle-left) L3C Aquarius; (middle-right) L3C SMAP; (bottom) L3C SMOS. Each pixel represents the median value after a moving window over 2 pixels in latitude and time. Data which are significantly different from 0 (at 95%) are indicated with dots. All sub-figures share the same colour bar. ----- 41

Figure 14: Seasonal climatology of the gridded pairwise CCI L4 difference with Argo calculated using the median. A moving window average of 2 x 2 pixels in longitude and latitude have been applied to increase the number of sampled, hence the significance. Pixels, which are statistically significant (at 95%) are indicated with dots. ----- 42

Figure 15: Latitudinal band (20° wide) median of the gridded pairwise SSS difference between CCI and Argo from (top) to (bottom) of [40°N;60°N] to [40°S;60°S]. A yearly rolling average is further applied to the data. Curves are in (black) for L4v2; (green) L3 SMOS; (blue) L3 Aquarius; (Orange) L3 SMAP. ----- 43

Figure 16: Seasonal Salinity gradient (in pss/m) derived from Argo between 5m and 10m. Gradient are gridded on the same grid as used for the pairwise difference (bi-weekly; 175 km). ----- 45

Figure 17: STD of (left) high-pass (<5 months) filtered time series; (middle) annual cycle; (right) low-passed (>13 months) filtered time series of (1st row) CCI+SSS L4v3 data; (2nd row) ratio between 1st and 3rd row or equivalently between v3 and v1; (3rd row) CCI+SSS L4v1 data; (bottom row) ensemble in situ data. All data used the same time period up to 2018. ----- 46

Figure 18 : Average power spectrum of SSS from (black) moorings, (red) CCI weekly products stated in legend, (blue) ISAS, (pink) Mercator; from PiMEP. ----- 48

Figure 19: same as above but for the Monthly products. ----- 49

Figure 20: CCI+SSS on 30 June 2011 with 93 TSG transects in the Subtropical North Atlantic (dashed) and 26 TSG transect in the Tropical Atlantic. ----- 51

Figure 21: a) Density spectra from from 88 collocated TSG (black); CCI+SSS v2.31 (dashed red); CCI+SSS v3.1 (solid red) SSS transects in Subtropical North Atlantic. Vertical thick black bar is the level of confidence at 95%. b) Coherency between the TSG and CCI+SSS SSS transects. Dashed line is the level of significance at 95%. c) Density spectra from from 26 collocated TSG (black)/CCI+SSS(red) SSS transects in Tropical Atlantic. Vertical thick black bar is the level of confidence at 95%. d) Coherency between the TSG and CCI +SSS SSS transects. Dashed line is the level of significance at 95%. ----- 53

Figure 22 : Time series of the normalised SSS normalised using (A) the satellite uncertainty; (B) the total uncertainty combining the sat and reference uncertainty. (1st row for each panels)

represent (solid line) the median and (dashed line) the mean. (last row for each panels) represent (solid line) the robust std and (dashed line) the classic std. (colours) are for the L4v3 and L3C Aquarius, SMAP and SMOS data. -----55

Figure 23: measured standard deviation (green and red dots) for resp. classic and robust std; of the gridded pairwise CCI/Argo difference for each uncertainty bins. (top) using satellite uncertainty; (bottom) using total uncertainty - sat + ref. (column from left to right) for L4v3, L3 Aquarius, SMAP, SMOS. The size of the circle indicates the number of data. -----56

List of tables

Table 1 – Applicable documents (as seen in CCI+SSS website, http://cci.esa.int/salinity) -----	12
Table 2 – Reference documents-----	13
Table 3: Statistics of CCI L4 v2.3 30dr against in situ data for the global ocean applying criteria C1 (only pairs where RR=0mm/h, $3 < U < 12$ m/s, SST>5°C, distance to coast > 800km). From PiMEP	27
Table 4: Statistics of CCI products against Argo data for the global ocean for the same period covering 2010-01-01 to 2018-11-01. From PiMEP. -----	30
Table 5: Statistics of CCI products against Argo data for the global ocean applying criteria C1 (only pairs where RR=0mm/h, $3 < U < 12$ m/s, SST>5°C, distance to coast > 800km) for the same period covering 2010-01-01 to 2018-11-01. From PiMEP. -----	31
Table 6: Same as Table 4 but for the entire period of v3 and for the L3 and L4 products. -----	31
Table 7: Same as Table 5 applying criteria C1 on Argo but for the L3 and L4 products. -----	31



1 Introduction

1.1 Purpose and scope

The purpose of this document (D4.1 Product Validation and Intercomparison Report, PVIR, document version v3.0) is to describe the results of the validation of the Sea Surface Salinity (SSS) products obtained during the ESA CCI+ SSS project when compared with other data sources. The PVIR is a requirement of the Statement of Work (Task 3 SoW ref. ESA-CCI-PRGM-EOPS-SW-17-0032). The PVIR contains a list of all reference datasets used for validation of each SSS product.

This report contains an assessment of both the level 4 and level 3 (ascending, descending and combined ascending plus descending) products for weekly and monthly time periods. The products are based on a temporal optimal interpolation of SSS data measured by SMOS, Aquarius-SAC and SMAP satellite missions. All products are gridded on an equal area EASE-2 grid with a grid resolution of ~25 km.

1.2 Structure of the document

This document is composed of four sections:

Section 1 introduces the purpose and scope of the document. Section 2 provides an executive summary of the results presented. Section 3 presents the data and methods used for the systematic validation presented in Section 4. Supplementary material is provided in Annex A.

1.3 Applicable Documents

PSD	Product Specification Document	SSS_cci-D1.2-PSD-v1r6
PUG	Product User Guide	SSS_cci-D4.3-PUG-v1.1
PVP	Product Validation Plan	SSS_cci-D2.5-PVP-v1.1
SoW	CCI+ Statement of Work	SOW

Table 1 – Applicable documents (as seen in CCI+SSS website, <http://cci.esa.int/salinity>)



Climate Change Initiative+ (CCI+)
Phase 1
Product Validation and
Intercomparison Report

Ref.: ESA-CCI-PRGM-EOPS-SW-17-0032
 Date: 9/12/2021
 Version : v3.0
 Page: 13 of 59

1.4 Reference Documents

ID	Document	Reference
RD01	Product Validation Plan	
RD02	Pi-MEP consortium, March 2019; Match-up database Analyses report, CCI-L4-ESA-MERGED-OI-V1.5-MONTHLY Argo Global Ocean: pimep-mdb-report_GO_cci-l4-esa-merged-oi-v1.5-1m_argo_20190315.pdf	
RD03	G. Reverdin, S. Morisset, L. Marié, D. Bourras, G. Sutherland, B. Ward, J. Salvador, J. Font, Y. Cuyppers, L.R. Centurioni, V. Hormann, N. Koldziejczyk, J. Boutin, F. D’Ovidio, F. Nencioli, N. Martin, D. Diverres, G. Alory & R. Lumpkin (2015). Surface salinity in the North Atlantic subtropical gyre during the STRASSE/SPURS summer 2012 cruise. <i>Oceanography</i> 28 (1): 114-123	
RD04	N. Hoareau, A. Turiel, M. Portabella, J. Ballabrera-Poy & J. Vogelzang (2018). Singularity Power Spectra: A Method to Assess Geophysical Consistency of Gridded Products - Application to Sea-Surface Salinity Remote Sensing Maps. <i>IEEE Transactions on Geosciences and Remote Sensing</i> 56, 5525-5536	
RD05	Product Validation and Intercomparison Report version 2	
	Stammer et al., 2020, How good do we know ocean salinity and its changes?, submitted to <i>Progress in Oceanography</i>	Stammer et al., 2020
	Boutin et al 2016 , Satellite and In Situ Salinity: Understanding Near-surface Stratification and Sub-footprint Variability, <i>Bulletin of American Meteorological Society</i> , 97(10), doi: 10.1175/BAMS-D-15-00032.1	Boutin et al 2016
	Supply, A., J. Boutin, J.-L. Vergely, N. Kolodziejczyk, G. Reverdin, N. Reul, and A. Tarasenko (2020), New insights into SMOS sea surface salinity retrievals in the Arctic Ocean, <i>Remote Sensing of Environment</i> , 249, 112027, https://doi.org/10.1016/j.rse.2020.112027 .	Supply et al, 2020a
	Supply, A., J. Boutin, G. Reverdin, J.-L. Vergely, and H. Bellenger, 2020: Variability of satellite sea surface salinity under rainfall. In: <i>Satellite Precipitation Measurement</i> , V. Levizzani, C. Kidd., D. B. Kirschbaum, C. D. Kummerow, K. Nakamura, F. J. Turk, Eds., Springer Nature, Cham, <i>Advances in Global Change Research</i> , 69, 1155-1176, https://doi.org/10.1007/978-3-030-35798-6_34 .	Supply et al, 2020b

Table 2 – Reference documents



Climate Change Initiative+ (CCI+)
Phase 1
Product Validation and
Intercomparison Report

Ref.: ESA-CCI-PRGM-EOPS-SW-17-0032
Date: 9/12/2021
Version : v3.0
Page: 14 of 59

1.5 Acronyms

CAR	Climate Assessment Report
CCI	The ESA Climate Change Initiative (CCI) is formally known as the Global Monitoring for Essential Climate Variables (GMECV) element of the European Earth Watch programme
CCI+	Climate Change Initiative Extension (CCI+), is an extension of the CCI over the period 2017–2024
CMEMS	Copernicus Marine Environmental Monitoring Service
EASE-2	Cylindrical Equal Area Scalable Earth grid 2.0
ECMWF	European Centre for Medium Range Weather Forecasts
ECV	Essential Climate Variable
FRM	Fiducial Reference Measurements
ISAS	In-Situ Analysis System
ISDB	in situ database (of Fiducial Reference Measurements and satellite measurements)
MDB	Match-up DataBase
Pi-MEP	Pilot Mission Exploitation Platform
PSD	Product Specification Document
PUG	Product User Guide
PVIR	Product Validation and Intercomparison Report
PVP	Product Validation Plan
QA4EO	Quality Assurance Framework for Earth Observation
RFI	Radio Frequency Interference
SMAP	Soil Moisture Active Passive [mission of NASA]
SMOS	Soil Moisture and Ocean Salinity [satellite of ESA]
SoW	Statement of Work
SSS	Sea Surface Salinity
TSG	ThermoSalinoGraph
URD	User Requirements Document



2 Executive Summary

2.1 Sea Surface Salinity products

The products validated are:

For L4:

ESACCI-SEASURFACESALINITY-L4-SSS-MERGED_OI_Monthly_CENTRED_15Day_25km-
xxxxxxxx-fv3.2
ESACCI-SEASURFACESALINITY-L4-SSS-MERGED-OI-Weekly-CENTRED-1Day-25km-xxxxxxxx-
fv3.2

For L3:

ESACCI-SEASURFACESALINITY-L3C-SSS-
SMOSSMAPAQUARIUS_A_Monthly_Centred_15Day_25km-xxxxxxxx-fv3.2
ESACCI-SEASURFACESALINITY-L3C-SSS-
SMOSSMAPAQUARIUS_D_Monthly_Centred_15Day_25km-xxxxxxxx-fv3.2
ESACCI-SEASURFACESALINITY-L3C-SSS-
SMOSSMAPAQUARIUS_Monthly_Centred_15Day_25km-xxxxxxxx-fv3.2
ESACCI-SEASURFACESALINITY-L3C-SSS-SMOSSMAPAQUARIUS_A_Weekly-CENTRED-1Day-
25km-xxxxxxxx-fv3.2
ESACCI-SEASURFACESALINITY-L3C-SSS-SMOSSMAPAQUARIUS_D_Weekly-CENTRED-1Day-
25km-xxxxxxxx-fv3.2
ESACCI-SEASURFACESALINITY-L3C-SSS-SMOSSMAPAQUARIUS_Weekly-CENTRED-1Day-25km-
xxxxxxxx-fv3.2

Full description of the dataset can be found in the Product User Guide (PUG). The products follow recommendations of the Product Specification Document (PSD).

2.2 Main results

- In situ reference dataset derived from Argo floats upper salinity measurements (see details in section 3.1 below); Limited CCI data in the Arctic and Southern Ocean;
- Limited CCI data in the Arctic and Southern Ocean;
- No systematic biases against reference data found (see details in summary for PIMEP match-up report in section 2.3 below for more details);
- Global precision against reference gridded data is of 0.14;
- CCI version 3 products show slightly better performance than previous versions;
- Bay of Bengal: Similar performance between v1 and v3 against in situ, but v3 goes closer to the coast;
- Gulf of Guinea: Good agreement of CCI v2 against TSG and Argo/CTD with insignificant biases;
- Coherent variability between CCI v3 and in situ data
 - more coherent small-scale high-frequency variability for CCI;



Climate Change Initiative+ (CCI+)
Phase 1
Product Validation and
Intercomparison Report

Ref.: ESA-CCI-PRGM-EOPS-SW-17-0032
Date: 9/12/2021
Version : v3.0
Page: 16 of 59

- coherent annual amplitude signal;
- larger amplitude in the inter-annual variability for CCI but smaller than v1;
- Good agreement between CCI and reference data, including long-term stability, differences within 0.05 pss for latitudinal band between [40°S-20°N];
- Remaining seasonal oscillation of CCI SSS differences against reference before 2015:
 - CCI are fresher/saltier in Winter/Summer than reference;
 - Amplitude is maximum at high latitudes (40°-60°) and can exceed 0.1 pss peak-to-peak;
 - Amplitude is stronger for L3 SMOS;
- CCI SSS is lower than reference data in the beginning of the time series (2010) with an amplitude up to 0.1 pss;
- Mesoscale features in Tropical Atlantic are coherent between CCI v2, v3 and TSG transects up to a wavelength of 250-300km (features of ~150km);
- Uncertainty provided in CCI product are in good agreement with observations (within 30%).

2.3 Main results from Pi-MEP match-up reports

- No global bias found against Argo except for filtered collocations where:
 - SSS less than 33 pss (CCI saltier by 0.05 pss);
 - Mixed layer depth shallower than 20m (CCI saltier by 0.04 pss);
 - SSS higher than 37 pss (CCI fresher by 0.05 pss);
- Global precision (robust standard deviation; pairwise difference) against Argo of 0.16 pss
 - Decreasing to 0.13 pss for optimal region (>800 km from the coast; area with temporal standard deviation smaller than 0.2 pss);
 - Increasing to 0.2 pss for area characterised by one of the following conditions: rain and low wind; mixed layer depth <20m; area with temporal standard deviation >0.2pss;
 - Increasing to 0.24/0.23 pss for area closer than 150 km from the coast or with SSS < 33 pss, but these numbers also contain differences due to the different type of sampling by Argo and satellite;
- Comparison with other 29 satellite SSS products against Argo
 - CCI products have the best precision (and no bias) except for Aquarius L4 IPRC v5 products.
 - Surprisingly, same precision and correlation for the monthly and weekly products.
- Good agreement between the observed CCI product SSS power spectra and mooring for the two averaging period (weekly and monthly).



Climate Change Initiative+ (CCI+)
Phase 1
Product Validation and
Intercomparison Report

Ref.: ESA-CCI-PRGM-EOPS-SW-17-0032

Date: 9/12/2021

Version : v3.0

Page: 17 of 59

2.4 Recommendations and caveats to use CCI+SSS dataset

CAVEATS

- Products have not been fully optimised for some issues encountered at very high latitudes (i.e. ice, RFI, biases due to land-sea contamination).
- There is a systematic global underestimation (0.1 pss) of SSS starting at the beginning of the dataset, and gradually disappearing at the end of 2010.
- There is a seasonal varying bias (~0.1, peaking in the middle of the year) at high latitude and which decreases after 2015.



3 Validation: Data & Methods

This section describes the Data and Methods used for the main validation results given in section 4.

Following PVP [RD1] recommendations, the reference dataset used for product validation is based on:

- In situ measurements of close-to-surface (<10 m) Argo from Pi-MEP

The reasoning for this choice of reference dataset is as follows:

- In the list of acceptable Fiducial Reference Measurements (FRM) referred to in PVP [RD1], the Argo dataset has been selected as it is the only dataset to provide regularly an almost complete coverage of global open water ocean. The temporal distribution from 2010 is also homogeneous [Pi-MEP – RD2].

In the following, the Argo dataset is described with its collocation criteria along with the gridding method and the method to estimate representativeness errors and validate uncertainties. A summary of the spatial (horizontal) representativeness error of in situ measurement, as described in the PVP [RD1], is given here. Finally, quality metrics to assess CCI products are presented.

The weekly products use monthly fields on which observed variability is added, therefore the focus of this summary report is on monthly fields, unless mentioned otherwise. We report in this document on validation against other in situ dataset (TSG, drifters, mammal measurements) which are provided on the Pi-MEP platform. Description of these datasets and full validation of Weekly and Monthly fields are available on the Pi-MEP platform:

- <https://pimep.ifremer.fr/diffusion/analysis/>
- <ftp://ftp.ifremer.fr/ifremer/cersat/pimep/diffusion/analysis/>

3.1 Dataset description

3.1.1 Argo match-ups database: Pi-MEP MDB

The Argo floats used for validation have been taken from Pi-MEP where quality control checks have been made. The text below is an extract of the detailed description of the Argo dataset and of the collocation (Match-ups Data Base - MDB) with CCI+SSS products.

Argo is a global array of 3,000 free-drifting profiling floats that measure the temperature and salinity of the upper 2000 m of the ocean. This allows continuous monitoring of the



Climate Change Initiative+ (CCI+)
Phase 1
Product Validation and
Intercomparison Report

Ref.: ESA-CCI-PRGM-EOPS-SW-17-0032

Date: 9/12/2021

Version : v3.0

Page: 19 of 59

temperature and salinity of the upper ocean, with all data being relayed and made publicly available within hours of collection. The array provides around 100,000 temperature/salinity profiles per year distributed over the global open water oceans at an average of 3-degree spacing. Only Argo salinity and temperature float data with a quality index set to 1 or 2 and data mode set to real time (RT), real time adjusted (RTA) or delayed mode (DM) are considered in Pi-MEP. Argo floats that may have problems with one or more sensors appearing in the grey list maintained at the Coriolis/GDACs are discarded. Furthermore, Pi-MEP provides an additional list of ~1000 "suspicious" Argo salinity profiles that are also removed before analysis. The upper ocean salinity and temperature values recorded between 0 m and 10 m depth are considered as Argo sea surface salinities (SSS) and sea surface temperatures (SST). These data were collected and made freely available by the international Argo project and the national programs that contribute to it [Argo (2000)].

The Argo MDB is produced from the previously described cleaned Argo dataset. For the monthly CCI+SSS product, the match-up temporal window radius is 7.5 days around the central date of each satellite time step (bi-weekly, monthly averaged), and 12.5 km for the spatial window radius for each grid nodes centre of a 25 km spatial resolution product. If several satellite pixels are found to meet these criteria, the final satellite SSS match-up point is the closest in time from the in situ data measurement date. The final spatial and temporal lags between the in situ and satellite data are stored in the MDB files. A wide range of collocated auxiliary information are also provided in the MDB.

All the data are freely available as NetCDF files at:

- <https://pimep.ifremer.fr/diffusion/data/>
- <ftp://ftp.ifremer.fr/ifremer/cersat/pimep/diffusion/data/>

This MDB is used as it is in all Pi-MEP reports, and it will be specified if the context is different from the one described below.

3.1.2 Reference dataset: gridded MDB

Typically, Argo floats sample the water column every 10 days. In order to study some specific processes with strong temporal variability, some Argo floats profile the water column up to every 2 hours. The floats tend to be located in areas where SSS variability is strong and artificially increase the number of collocations in these specific areas. Consequently, it degrades comparison against satellite based SSS. To solve this issue, only the median value for each grid point of all pairwise Pi-MEP MDB values is taken. The same biweekly temporal sampling as CCI monthly products is used. The spatial sampling is subsampled by a factor 7 both in latitude and longitude in order to get enough data for a given pixel over the full time series. The spatial grid corresponds to a 175 km Equal Area EASE grid.

This gridded MDB is used as the reference dataset except if specified otherwise.



3.2 Uncertainty validation

To validate satellite uncertainty estimates, the approach is to compare the distribution of the difference of satellite SSS minus reference SSS ($\Delta SSS = CCI - ref$). In an ideal scenario, the ΔSSS temporal standard deviation equals the pixel-based satellite uncertainty ($\Delta\sigma_{sat}$):

$$\sigma_{\Delta SSS=CCI-ref} = \Delta\sigma_{sat}$$

However, as stated in the PVP [RD1] the geophysical variability of reference SSS data over the time-space scale of remote sensing products depends not only on the particular spatial resolution and time window defining the remote sensing products, but also on the region at which this variability is estimated (inter-regional variability being quite significant [RD3]). Consequently, the ΔSSS standard deviation is a combination of both the satellite SSS uncertainty and the uncertainty in the reference SSS ($\Delta\sigma_{ref}$):

$$\sigma_{\Delta SSS} = \sqrt{\Delta\sigma_{sat}^2 + \Delta\sigma_{ref}^2}$$

In the reference uncertainty all the following terms are included:

- $\Delta\sigma_{meas.}$: Measurement uncertainty (direct ground-truth instrument error);
- $\Delta\sigma_{space}$: Spatial representativeness error (difference in spatial sampling of a point measurement versus a surface measurement defined by a grid cell);
- $\Delta\sigma_{time}$: Time representativeness error;
- $\Delta\sigma_{vertical}$: Vertical representativeness error (difference in depth of the measurements).

The reference uncertainty corresponds to the following combination:

$$\Delta\sigma_{ref} = \sqrt{\Delta\sigma_{space}^2 + \Delta\sigma_{time}^2 + \Delta\sigma_{vertical}^2 + \Delta\sigma_{meas.}^2}$$

In the following, we assume the measurement uncertainty to be negligible ($\Delta\sigma_{meas.} = 0$). This is true at first order as we consider all poor measurements to have been discarded with the quality control and filtering methods applied by Pi-MEP.

The vertical representativeness error, will be discussed in section 4.3. Although sometimes important, it is neglected for now ($\Delta\sigma_{vertical} = 0$). The time representativeness error, although sometimes important (e.g. river plumes), is not considered for now ($\Delta\sigma_{time} = 0$). Argo measurements have been selected in a +-7.5 days range around the central date of each satellite time step with a 30 days/monthly running mean. The spatial representativeness error is the only remaining reference uncertainty considered in this uncertainty assessment. This



error is fully described in the PVP [RD1], a summary is provided below. The spatial power spectra of SSS consistently exhibits a spectral slope of -2.4 ($S(k)=\beta k^{-2.4}$) in a range going from a few kilometres to basin scale ($\sim 10,000$ km) [RD4]. The variance contained between the spatial frequency k_L and k_l (respectively, between the scales l and L , with $l < L$) is given by the double integral:

$$S^2(k_L, k_l) = \iint_{k_L < k < k_l} d\mathbf{k} S(\mathbf{k}) = B \int_{k_L}^{k_l} k dk k^{-2.4}$$

Assuming three spatial scales: g for the ground truth measurements, r for the remote sensing product and L for the basin scale, $g \ll r \ll L$, $\sigma_0 = \sigma(r)$ the standard deviation of SSS contributed by all scales as measured by remote sensing, we obtain the following relationship:

$$DS^2(g, r) \approx S_0^2 \left(\frac{r}{L}\right)^{0.4} \approx S^2(r) \left(\frac{r}{L}\right)^{0.4}.$$

Assuming $L = 5000$ km, with $r = 25$ km for the SSS product, the spatial representativeness is estimated as follow:

$$\Delta\sigma_{space} = \sigma_0 * 0.35$$

With $\sigma_0 = \sigma(r)$ the CCI SSS field temporal standard deviation in time for each grid cell.

3.3 Quality metrics

Two types of quality metrics have been used throughout this document:

- Standard statistics: **mean** and **standard deviation (std)**. It assumes the central limit theorem can be relied on to produce normally distributed estimates;
- Robust statistics based on ranking which are robust against deviation from a normal distribution assumption: **median** and a robust standard deviation (**std***) scaled from the InterQuartile Range (IQR) by a factor 27/20 assuming a normal distribution.

PVP [RD1] recommends to discard statistics with less than 30 samples. In the following, two approaches have been followed. If one can estimate significance of an hypothesis (e.g. bias), values which are significant at 95% are indicated with dots. For standard deviation, where there is no related hypothesis, data calculated with less than 30 samples are indicated with hatching. Mean and median are significant for values higher than 1.96 (at 95%) the standard error of mean and median respectively. The confidence interval estimate for the mean and



Climate Change Initiative+ (CCI+)
Phase 1
Product Validation and
Intercomparison Report

Ref.: ESA-CCI-PRGM-EOPS-SW-17-0032
Date: 9/12/2021
Version : v3.0
Page: 22 of 59

median follow the same approach. The confidence interval estimate for the standard deviation and the robust standard deviation based on IQR use a random resampling of the data (python astropy.stats.bootstrap method).. For readability, the number of figures has been restricted and limited, when necessary, to the robust statistics (median and robust standard deviation based on IQR) which are more representative of the majority of the distribution.

Standard Error of the Mean is estimated following:

$$sem = \frac{\sigma}{\sqrt{N}}$$

Standard Error of the Median is estimated following:

$$sem_{median} = \frac{\sigma}{\sqrt{\frac{2(N+2)}{\pi}}}$$



4 Validation of Products, Stability, Resolution and Product Uncertainty Estimates

In this section, we present a systematic validation with a focus on the CCI L4 version 3 product. It will be compared to the CCI L4 v2 and v1 and to the v3 L3 (ascending, descending, combined) products. Section 4.1 describes the accuracy and precision of the products, including the case studies of validation in the Bay of Bengal and in Congo plume; section **Error! Reference source not found.** analyses their stability and section 4.3 analyses the in situ vertical representativeness error. The effective temporal and spatial resolution are assessed in section 4.4 and includes the case studies of SSS temporal variability at different time scale and of the mesoscale features in Tropical Atlantic. The quality of uncertainty estimation is assessed in section 4.5.

4.1 Accuracy & Precision

4.1.1 Products validation for L4

SSS are presented in the top panels of *Figure 1* centred on 15th of January 2015 for the CCI+SSS monthly product and all Argo profiles top measurements. Although the two subplots of the top panel are difficult to compare, Argo profiles are point wise measurements and CCI provides an SSS field, there is a good agreement between the two sets of observations. The satellite derived product enables accurately mapping the gradient which is difficult with Argo point measurements. The subplots in middle panel represent the temporal median of CCI and of the gridded MDB. There is very good agreement in the resolved patterns between the two fields. In the gridded MDB field, some areas are insufficiently sampled (less than 30 grid points) particularly in some coastal areas affected by river plumes (e.g. Amazon) or enclosed seas (e.g. Caribbean Sea, maritime continent, Mozambique channel), and in the open ocean in the middle of the subtropical gyres or at high-latitude (Arctic and Southern oceans). The temporal variability observed by CCI and Argo is represented on the subplots at the bottom of using the robust standard deviation. The high variability regions (e.g. in the vicinity of the Amazon and Congo plumes, in the Indian ocean, the ITCZ, or the Gulf stream) are well observed in both the CCI and gridded MDB. However, the high variability observed at high latitudes (e.g. Brazil-Malvinas Convergence Zone, Agulhas return current, Gulf Stream) with Argo floats is not totally reproduced by the CCI products. Part of this SSS variability might occur at finer spatial resolution than sampled by the satellites (<50 km) and this effect is expected to be more present at high latitude were mesoscale is at finer scale than at low latitudes. Over most of the polar regions no CCI data are available (*Figure 2*) as most of the data have been rejected in the processing. Polar regions were not the focus of this first phase of CCI data.

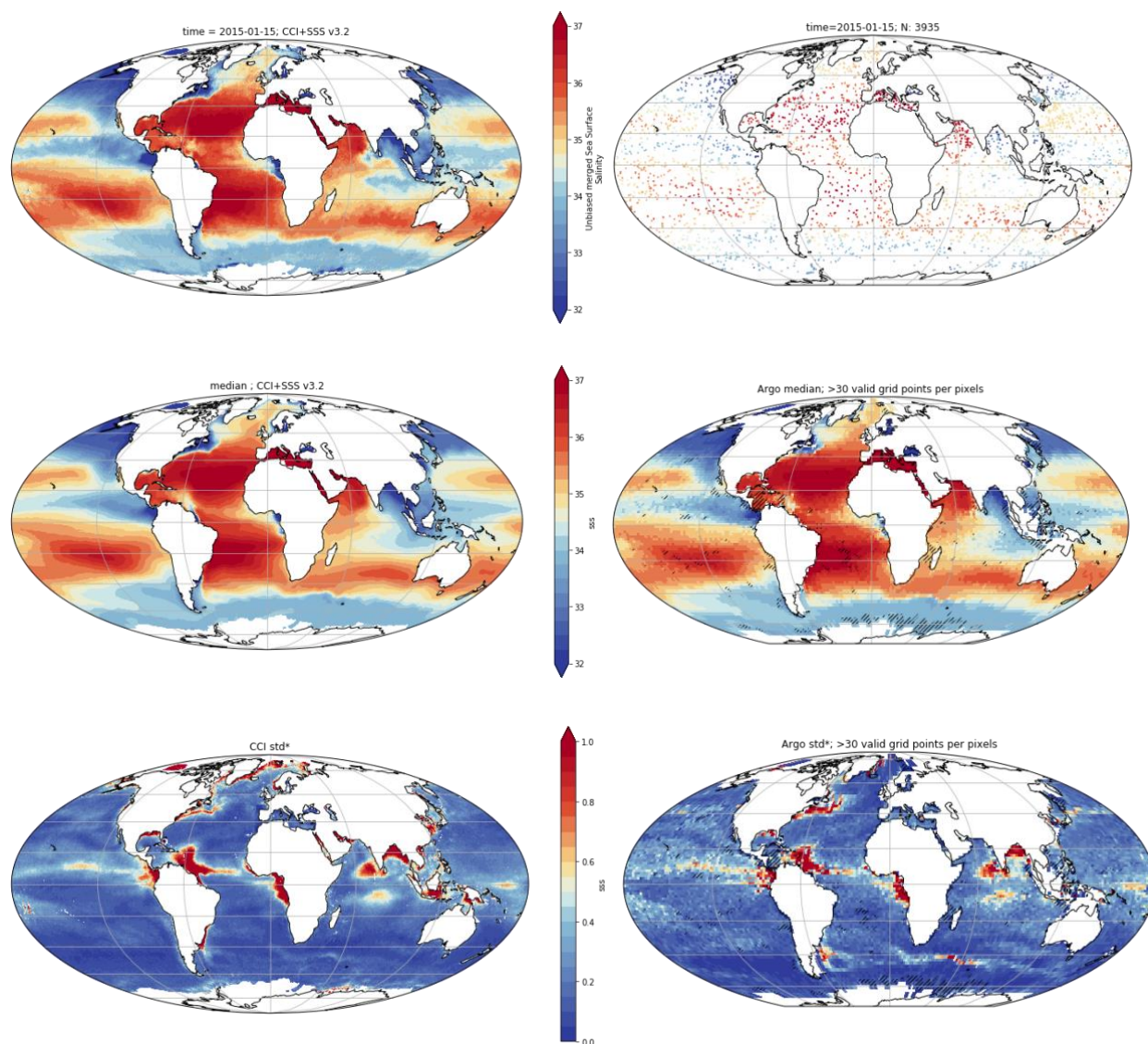


Figure 1: (top-left) L4 CCIv3 monthly SSS for the 15th of January 2015, (top-right) Argo floats upper salinity measurements from the Pi-MEP MDB for the month of the 15th of January 2015. (middle/bottom-left) temporal median/robust standard deviation of L4 CCIv3 SSS. (middle/bottom-right) temporal median/robust standard deviation of the gridded MDB SSS. Dashed lines indicates pixel with less than 30 points over the full time-series.

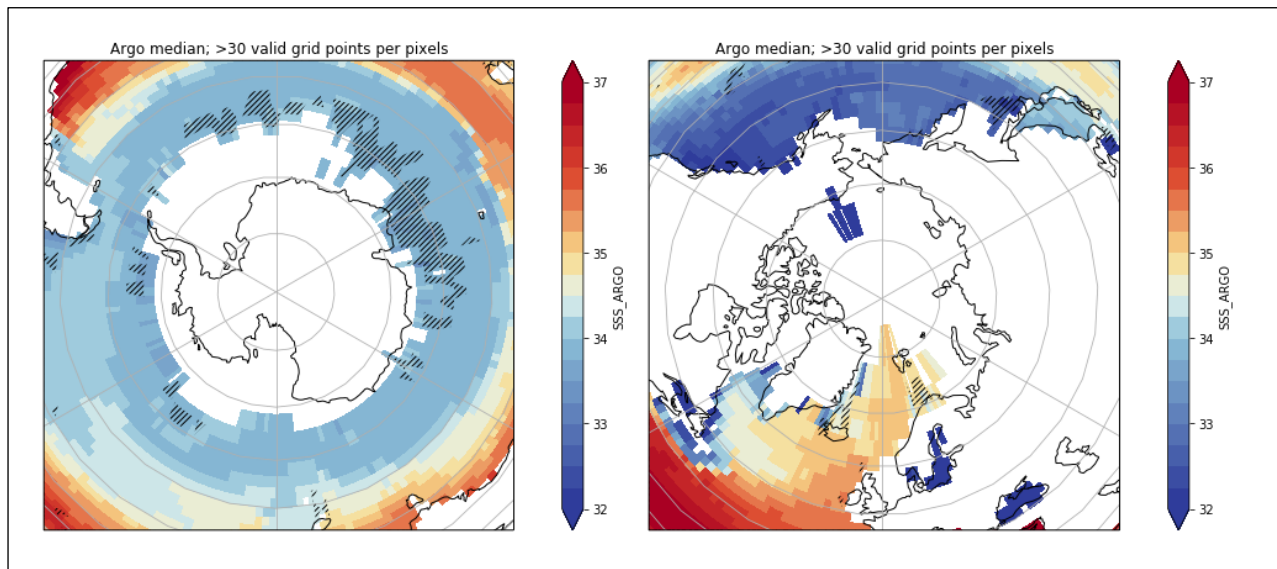


Figure 2: Same as Figure 1 middle-right but centred around the poles.

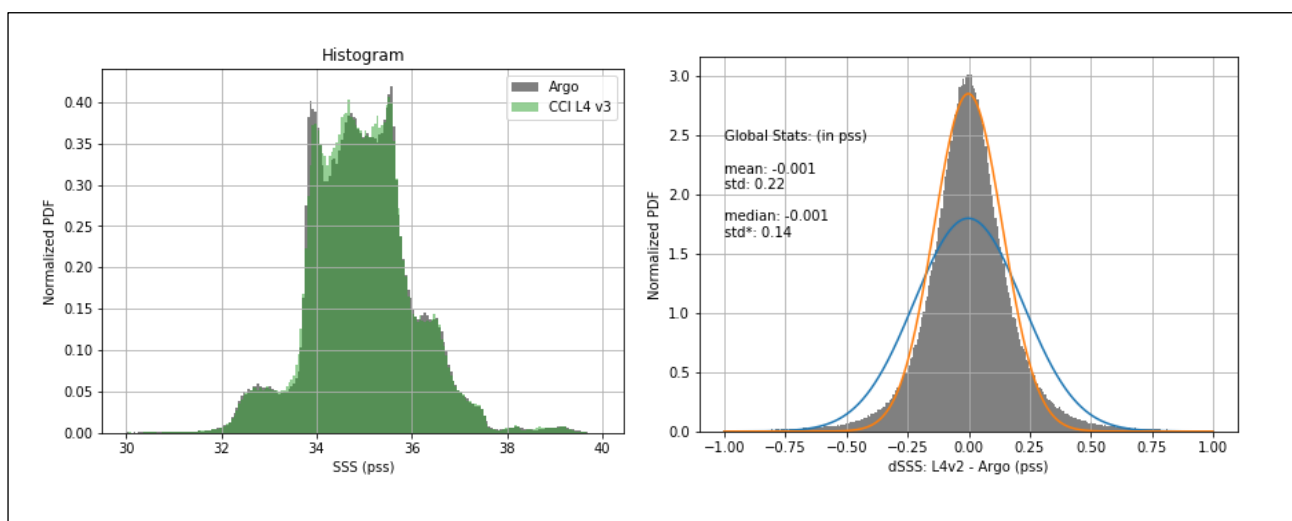


Figure 3: Histogram of all pairwise gridded MDB (left) Argo SSS in grey and CCI L4 v3 SSS in green; (right) Gridded MDB of the CCI L4 v3 minus Argo difference, (blue line) normalized probability function (PDF) using computed mean and std, (orange curve) normalized PDF using computed median and robust std.

The distributions of the gridded MDB of pairwise CCI L4 and Argo SSS are very similar (Figure 3-left) over the full range of SSS from 30 pss to 40 pss. The peak of distribution close to 34 pss is better resolved for CCI L4 v3 compared to previous CCI L4 v2 [RD05]. The distribution of the gridded MDB of pairwise CCI difference against Argo (Figure 3-right) highlights the absence of systematic bias (not significant at 5%), and a robust std of 0.14 pss (0.22 pss for the classic std). This difference between the robust and classic std is due to the non-normal distribution of the data difference (longer tails). The gridded pairwise measurements of Argo and CCI



Climate Change Initiative+ (CCI+)
Phase 1
Product Validation and
Intercomparison Report

Ref.: ESA-CCI-PRGM-EOPS-SW-17-0032
Date: 9/12/2021
Version : v3.0
Page: 26 of 59

present a square of the Pearson correlation coefficient (R^2) of 98%. These statistics are better than the previous CCI L4 v2 version [RD05].

Pi-MEP statistics against Argo DM for L4 v1.8, v2.3 and v3.2 (Pi-MEP MDB) covering the exact same period from 01 January 2010 to 01 November 2018, are summarised in Table 4 and Table 5 for the weekly and monthly products (with PiMEP C1 collocation conditional criterion – no rain, moderate wind, $SST > 5^\circ\text{C}$, distance to coast $> 800\text{km}$). Despite covering the same time period, the number of collocations slightly differs between versions. This small difference is due to flag differences amongst versions of CCI products.

For the weekly products (1st three rows in Table 4), there is a constant improvement of the statistics against all Argo DM collocations between versions. The standard deviation improves (both robust and classic std) by about 10% to 15% especially between v2.3 and v3.2 with values reaching 0.15 pss. Biases stay low for the three versions, but it appears a small bias for version 3 on this sub-selected period [2010-1018]. The explained variance (R^2) is very high with values around 0.97 for the three versions. The fraction of variance unexplained ($FVU = 1 - R^2$) degrades between v2.3 and v1.8 by about 20%, then for version 3 by an improvement of about 40% against v2. The number of collocations between v1.8 and v3.2 decreases by about 1% indicating a slightly more restrictive flagging procedure.

For the monthly products against all Argo DM (last three rows in Table 4), statistic improvement is relatively limited between the three versions compared to the progress for the weekly products. The standard deviation improves at most by 10% up to 0.16 pss. The v3 monthly precision (std and std*) surprisingly does not reach an as good precision as the v3 weekly. This suggests that the ground truth representativeness error in time plays a significant role in the precision evaluation. Despite this, the v3 monthly product explains more variance than v2 (-40% of fraction of variance unexplained) and v1 (-30% of FVU). V3 also gets about 2% more collocations against Argo than v2 or v1, which is opposite to what happens to the weekly products. Table 6 and Table 7 give statistics of all CCI L3 and L4 products for version 3. Except against CCI L3 for Aquarius (but at lower spatial resolution), which shows similar r^2 values as L4, statistical performance are always better for the L4 products.

Pi-MEP statistics of CCI L4 v3 against TSG, drifters and mammal's data with the C1 criterion are reproduced in Table 3. The time series of CCI SSS in each pixel is calibrated by comparing a quartile of the statistical distribution of CCI SSS with the one of ISAS SSS (ISAS 2015 up to 2015 and ISAS NRT v6.2 afterwards). Whereas TSG and drifters data are included in ISAS NRT, they are fully independent from ISAS 2015 (Gaillard et al., 2015). ISAS 2015 only uses Argo, marine mammals, ITP and TAO-Triton-Pirata-Rama data.

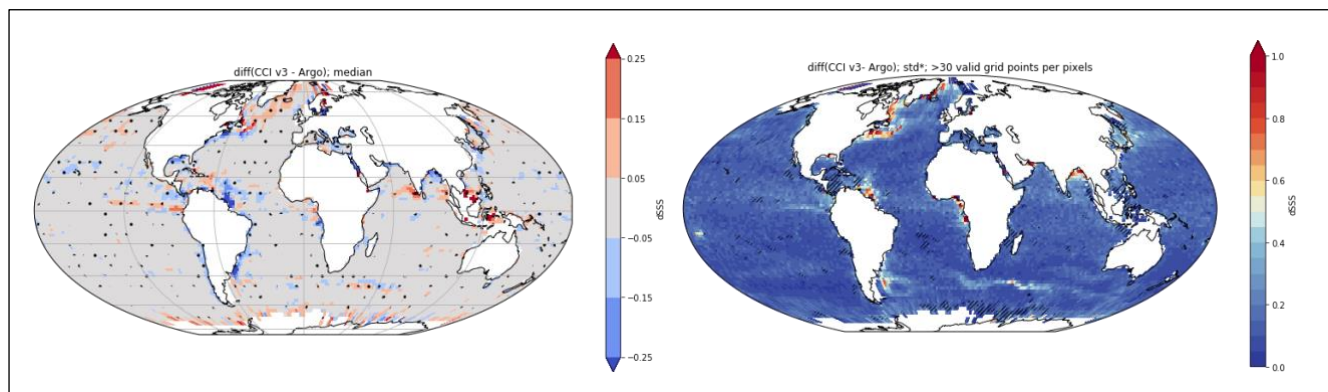


Figure 4 (left) Temporal median and (right) temporal robust standard deviation of gridded pairwise SSS differences between CCI and Argo. (on the left) A moving window of 2 pixels in longitude and latitude is applied to the median in order to highlight statistical significance (at 95%) which are indicated with dots. (on the right) Robust standard deviation calculated with less than 30 valid grid points in time are hatched.

To further assess the agreement between datasets, Figure 4 presents the temporal average (median) and the robust std of the gridded MDB of the pairwise differences between CCI and Argo. At large scale (open ocean), the median difference is predominantly within ± 0.05 pss and the robust std difference is below 0.2 pss. There is no large scale systematic spatial difference versus Argo. Whereas L4v2 was slightly fresher in the central Pacific Ocean (blue in Fig 3 of [RD05]), only small portions of the Pacific present significant fresh bias lower than 0.05 pss. Closer to the coast, major river plumes appear fresher (blue) in CCI. Close positive/negative differences are observed in the Gulf stream and Agulhas return current where meanders are common, suggesting differences between Argo and satellite sampling and spatial representativeness (pointwise measurement versus 50 km pixel). These higher discrepancies between CCI and in situ are also visible in the spread, with a temporal robust standard deviation of the differences higher than 0.4 pss at these fronts, in coastal areas and river plumes (Amazon plume, Bay of Bengal, ...).

Table 3: Statistics of CCI L4 v2.3 30dr against in situ data for the global ocean applying criteria C1 (only pairs where $RR=0\text{mm/h}$, $3 < U < 12\text{m/s}$, $SST > 5^\circ\text{C}$, distance to coast $> 800\text{km}$). From PiMEP

Insitu database	Nb	median	mean	std*	std	R2
Argo	303937	0.00	0.00	0.13	0.16	0.97
mammal	3023	-0.06	-0.05	0.19	0.23	0.87
drifter	835159	-0.02	0.01	0.13	0.22	0.98
tsg-legos-dm	442522	-0.02	-0.02	0.15	0.18	0.96
tsg-gosud-research-	321856	0.02	0.02	0.13	0.18	0.97
tsg-gosud-sailing-ship	161867	0.02	0.03	0.14	0.16	0.98
tsg-samos	1260556	0.03	0.06	0.18	0.25	0.94
tsg-legos-survostral	37796	0.02	0.01	0.15	0.16	0.54
tsg-ncei-0170743	87367	0.11	0.10	0.13	0.16	0.93
tsg-polarstern	28686	-0.02	-0.01	0.13	0.17	0.97



Climate Change Initiative+ (CCI+)
Phase 1
Product Validation and
Intercomparison Report

Ref.: ESA-CCI-PRGM-EOPS-SW-17-0032

Date: 9/12/2021

Version : v3.0

Page: 28 of 59

4.1.2 Products validation differences for Aquarius, SMAP, SMOS L3 products

In this subsection we will look at differences between CCI L3C v3 Aquarius, SMAP or SMOS products and CCI L4 v3. L3C products are simple grid averages of individual L2 satellite SSS after applying systematic corrections.

The temporal mean differences between CCI L3C SSS products and L4v3 do not highlight regions higher than 0.05 pss in absolute value except for the difference against SMOS where differences exceed 0.05 pss at high latitude and around Asia (Figure 5-top-left). The spread of L3C products versus L4 is generally below 0.1 pss except: for SMAP and Aquarius in areas of strong natural SSS variability or close to sea ice; and for SMOS, the spread exceeds 0.5 pss for most of the the Northern hemisphere in the vicinity (about 1,000 km) of the Asian, European and North-American continents, as well as in the vicinity of Antarctica (Figure 5-top-right).

The difference between ascending and descending passes does not show systematic differences higher than 0.05 pss for Aquarius and SMAP, but presents differences higher than 0.1 pss around Europe and Asia for SMOS (Figure 5-bottom-left). These differences have strongly improved compared to version 2 around North America [RD05]. Aquarius, does not produce strong differences between ascending and descending orbits, but there is an absence of data in some regions for ascending orbit which appear as white in Figure 5-bottom.

If one looks at the individual distributions of the gridded pairwise CCI L3C with Argo for each satellite, then none are able to reproduce the SSS distribution as measured by Argo floats (Figure 6), but CCI L4 combined products with a temporal OI are in very good agreement with Argo (Figure 3-left vs right).

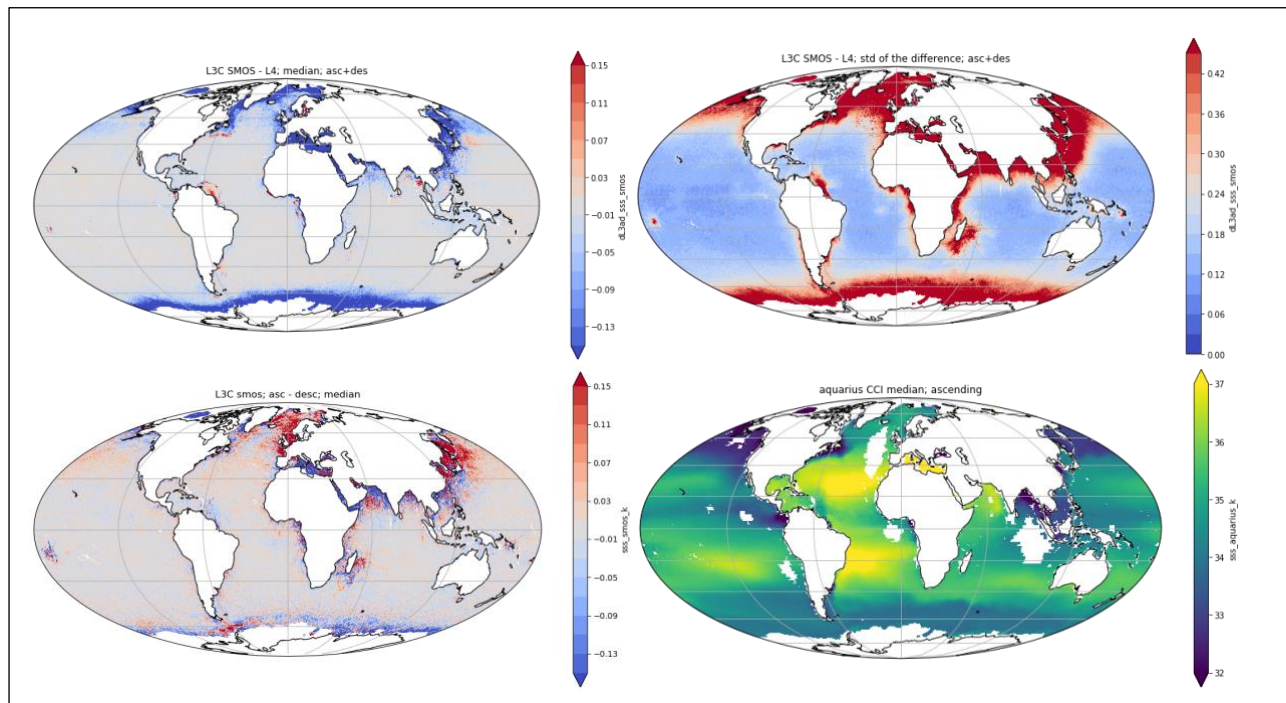


Figure 5: (top-left) temporal median of the CCI L3C SMOS difference against CCI L4 v3; (top-right) same but for the temporal std of the difference; (bottom-left) temporal median of the CCI L3C SMOS difference between Ascending and Descending passes; (bottom-right) temporal median of CCI L3C Aquarius SSS for ascending passes.

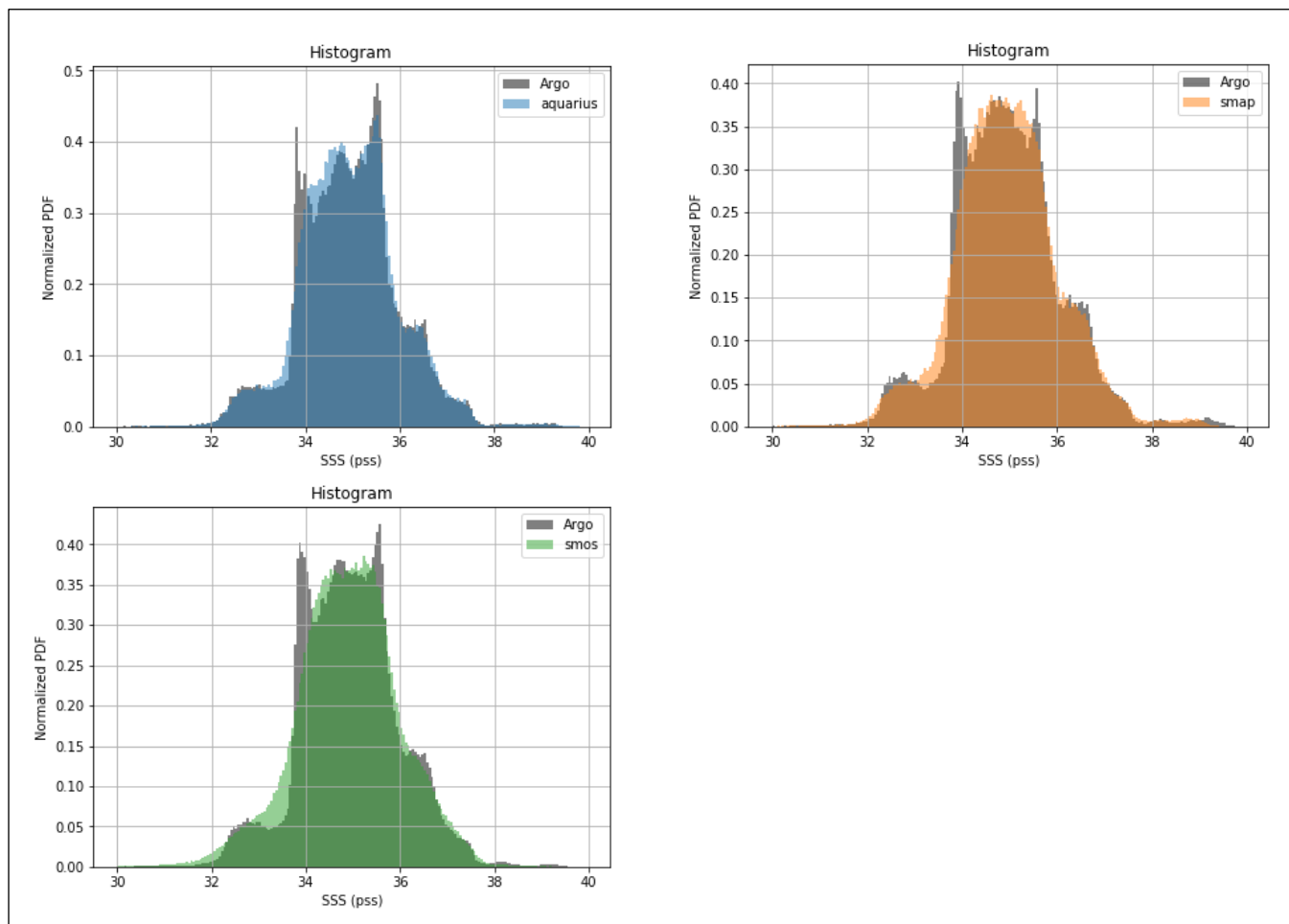


Figure 6: Normalised PDF of all CCI/Argo pairwise gridded MDB v3 for (grey) Argo, (blue) Aquarius, (orange) SMAP and (green) SMOS.

Table 4: Statistics of CCI products against Argo data for the global ocean for the same period covering 2010-01-01 to 2018-11-01. From PiMEP.

Satellite	Nb	median	mean	std*	std	R2
Weekly running average						
cci-l4-esa-merged-oi-v1.8-7dr	811224	0.00	0.00	0.17	0.29	0.969
cci-l4-esa-merged-oi-v2.3-7dr	808777	0.00	0.00	0.17	0.28	0.963
cci-l4-esa-merged-oi-v3.2-7dr	802840	-0.01	-0.01	0.15	0.24	0.977
Monthly running average						
cci-l4-esa-merged-oi-v1.8-30dr	802272	0.00	0.00	0.17	0.29	0.970
cci-l4-esa-merged-oi-v2.3-30dr	796822	0.00	0.00	0.16	0.28	0.964
cci-l4-esa-merged-oi-v3.2-30dr	813360	0.00	0.00	0.16	0.26	0.979



Climate Change Initiative+ (CCI+)
Phase 1
Product Validation and
Intercomparison Report

Ref.: ESA-CCI-PRGM-EOPS-SW-17-0032
 Date: 9/12/2021
 Version : v3.0
 Page: 31 of 59

Table 5: Statistics of CCI products against Argo data for the global ocean applying criteria C1 (only pairs where RR=0mm/h, 3<U<12m/s, SST>5°C, distance to coast > 800km) for the same period covering 2010-01-01 to 2018-11-01. From PiMEP.

Satellite	Nb	median	mean	std*	std	R2
Weekly running average						
cci-l4-esa-merged-oi-v1.8-7dr	273422	0.00	0.00	0.14	0.16	0.970
cci-l4-esa-merged-oi-v2.3-7dr	273771	0.00	0.00	0.14	0.17	0.969
cci-l4-esa-merged-oi-v3.2-7dr	272897	0.00	0.00	0.13	0.16	0.973
Monthly running average						
cci-l4-esa-merged-oi-v1.8-30dr	269599	0.00	0.00	0.13	0.17	0.969
cci-l4-esa-merged-oi-v2.3-30dr	269593	0.00	0.00	0.13	0.16	0.970
cci-l4-esa-merged-oi-v3.2-30dr	270151	-0.01	0.00	0.13	0.16	0.972

Table 6: Same as Table 4 but for the entire period of v3 and for the L3 and L4 products.

Satellite	Nb	median	mean	std*	std	R2
Weekly running average						
cci-l4-esa-merged-oi-v3.2-7dr	331614	0	0	0.13	0.19	0.961
cci-l3c-esa-aquarius-v3.2-7dr	115575	0	0	0.15	0.18	0.965
cci-l3c-esa-smap-v3.2-7dr	151577	0.01	0.01	0.3	0.32	0.894
cci-l3c-esa-smos-v3.2-7dr	328214	0	0	0.37	0.44	0.818
Monthly running average						
cci-l4-esa-merged-oi-v3.2-30dr	327631	0	0	0.13	0.18	0.964
cci-l3c-esa-aquarius-v3.2-30dr	113146	0	0	0.13	0.16	0.972
cci-l3c-esa-smap-v3.2-30dr	151887	0.01	0.01	0.18	0.2	0.954
cci-l3c-esa-smos-v3.2-30dr	322972	0	0	0.22	0.26	0.928

Table 7: Same as Table 5 applying criteria C1 on Argo but for the L3 and L4 products.

Satellite	Nb	median	mean	std*	std	R2
Weekly running average						
cci-l4-esa-merged-oi-v3.2-7dr	973110	0	0	0.16	0.25	0.977
cci-l3c-esa-aquarius-v3.2-7dr	332243	0	0.01	0.19	0.26	0.952
cci-l3c-esa-smap-v3.2-7dr	432321	0.01	0.01	0.34	0.4	0.932
cci-l3c-esa-smos-v3.2-7dr	923060	-0.01	-0.05	0.45	0.69	0.711
Monthly running average						
cci-l4-esa-merged-oi-v3.2-30dr	984595	0	0	0.15	0.27	0.982
cci-l3c-esa-aquarius-v3.2-30dr	331626	0	0.01	0.16	0.24	0.959
cci-l3c-esa-smap-v3.2-30dr	437073	0	0	0.21	0.29	0.965
cci-l3c-esa-smos-v3.2-30dr	923823	-0.01	-0.05	0.27	0.51	0.836

Biases of L3C Aquarius, SMAP and SMOS are indicated in Figure 7-left, with significant biases for both SMAP and Aquarius up to an order of +/-0.1 pss. On the contrary, SMOS does not present constant bias except in the Southern Ocean, Mediterranean Sea and Japan Sea. The

temporal standard deviation of the difference highlights strong differences with Argo for SMOS in the Labrador and Nordic Seas, in the Mediterranean Sea and around most of the coast in Asia.

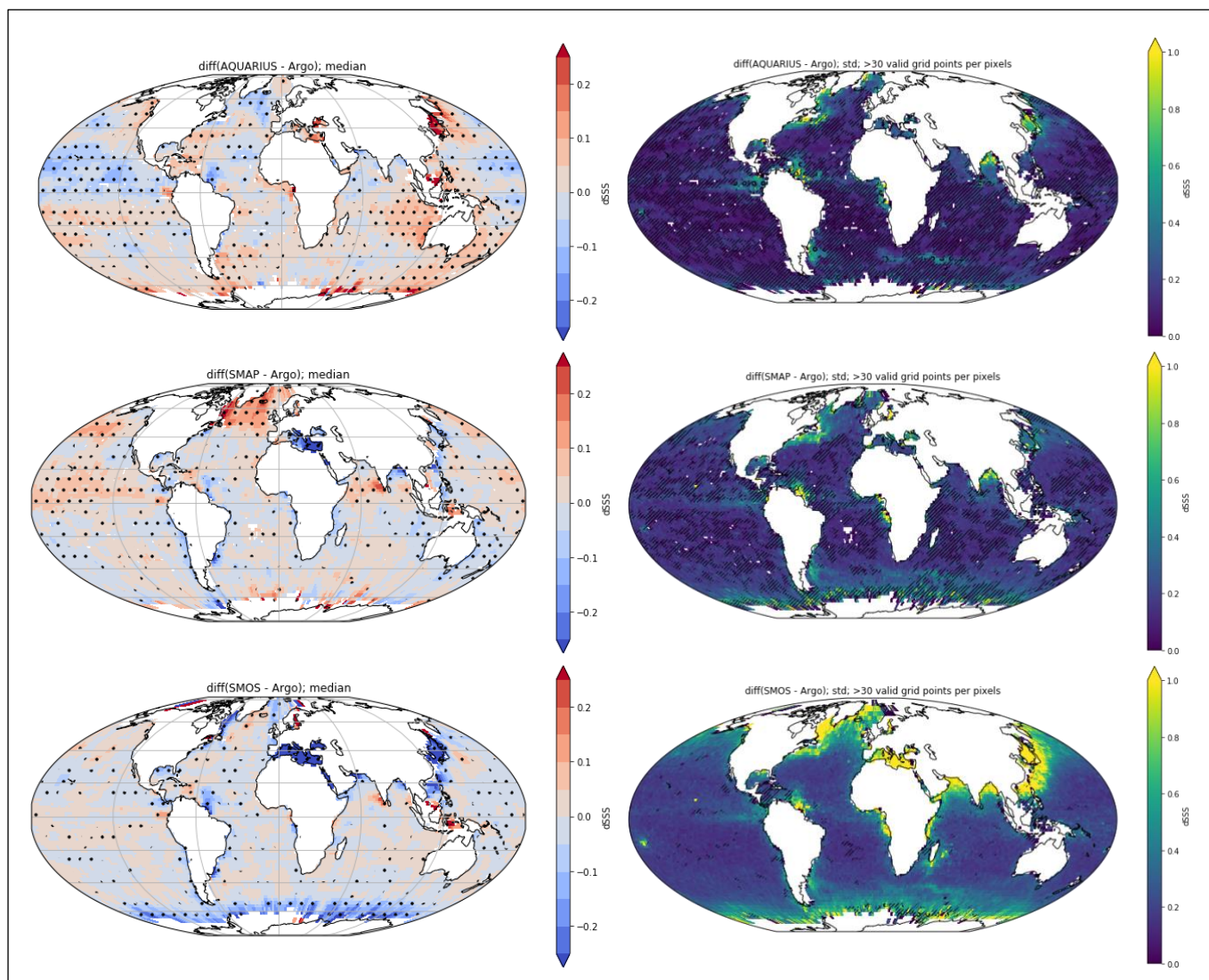


Figure 7: (left) temporal median of; (right) temporal classic std of the gridded MDB of the pairwise difference between CCI L3 combined asc+desc products and Argo for (top row) Aquarius; (second row) SMAP; (last row) SMOS. A moving window of 4 pixels in longitude and latitude is applied to the median (on the left) in order to highlight statistical significance (at 95%) which are indicated with dots. Std calculated with less than 30 valid grid points in time are hatched (on the right).

4.1.3 Validation in the Bay of Bengal (Case study 3: V.P. Akhil, J. Vialard)

The Bay of Bengal (hereafter, BoB) has large, seasonal freshwater inputs and an energetic circulation, including narrow coastal currents such as the EICC (East India Coastal Current) and a strong eddy variability. This creates large horizontal salinity gradients, which were previously difficult to study from available in situ data, sometimes resorting to fishermen

collecting water samples on the beach to monitor the seasonal expansion of the fresh, southward-flowing EICC (Chaitanya et al. 2014). While SMOS initially performed poorly in the Bay of Bengal (Akhil et al. 2016a), a reprocessing of the data has allowed major improvements (Boutin et al. 2018), yielding better performance compared to Aquarius and almost equivalent performance to that of SMAP (Akhil et al. 2020). The first release of the CCI project products also demonstrated performance which was at least equivalent to any of the individual SMOS, Aquarius or SMAP products over their common period (Akhil et al. 2020). Below, we briefly discuss the ongoing evaluation of the CCI v3 SSS product before reviewing pending issues that will be investigated in the near future.

Relative to the v1 product, v3 has applied a less stringent flagging to pixels that are near land (Figure 8). In the Bay of Bengal, this mostly impacts the spatial coverage near the Ganges-Brahma estuary, in the north of the Basin, and near the Andaman and Nicobar Islands, to the southeast.

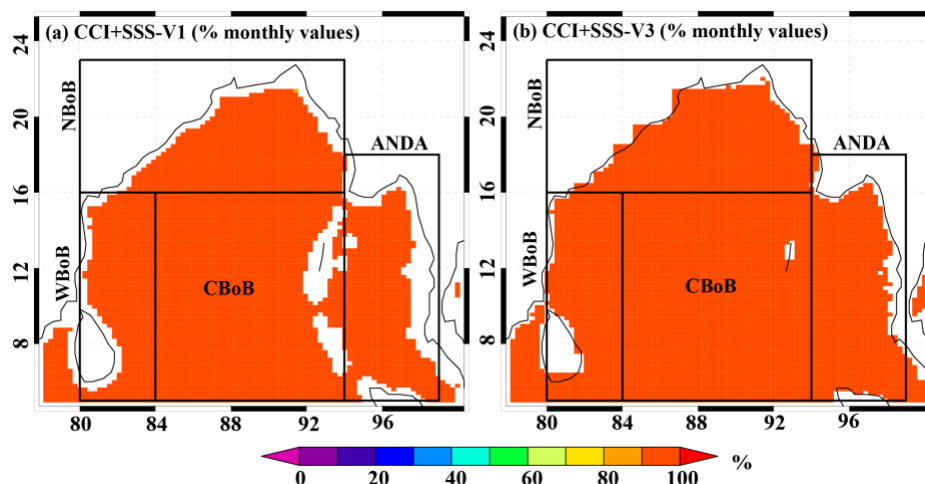


Figure 8: Spatial coverage of the CCI+SSS (a) v1 and (b) v3 products. The various boxes used for the comparison to in situ data of Figure 9 are marked.

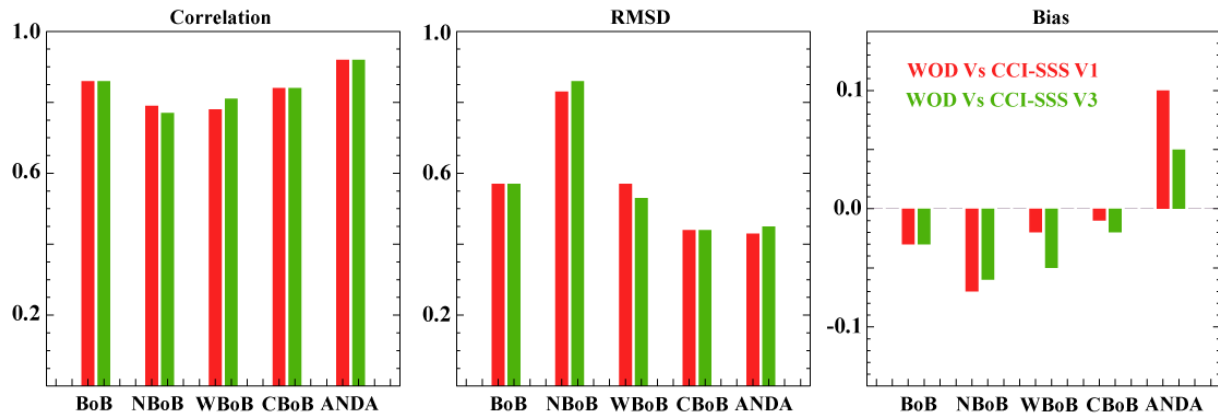


Figure 9: Correlation, root-mean square difference and bias of the CCI-SSS v1 (red) and v3 (green) products comparison to *in situ* data over the entire Bay of Bengal (BoB), and over the various regions indicated on Figure 8 (NBoB, WBoB, CBoB, ANDA). Only data points which are collocated with the two datasets have been considered, so that the two datasets are evaluated over the same sample.

Comparing the two datasets to the same *in situ* data sample (Figure 9) indicates that the v3 product is generally equivalent or slightly improved relative to the v1 product over most regions, except in the Northern Bay of Bengal (where the difference between the two datasets is weak). We will now need to specifically evaluate the additional data points in v3 close to the coast. Some preliminary analyses indicate that they tend to display a decreased performance relative to points in the open ocean, but that the signal to noise ratio is still favourable (i.e. that the standard error is still smaller than the amplitude of the variability in most regions).

4.1.4 Comparison in Congo Plume (Case Study 4: O. Houndegnonto, N. Kolodziejczyk, N. Reul)

The Gulf of Guinea (GG) is a key region for regional climate variability. A noticeable regional climate feature is the Western African Monsoon, which is strongly influenced by sea surface temperature and subsurface conditions in the Gulf of Guinea, including stratification, mixing and circulation. Large river runoff has strong impacts on the near surface thermohaline stratification and mixing in the Gulf of Guinea. In return, the river plume extensions are strongly influenced by seasonal and interannual wind driven surface circulation. In the eastern Gulf of Guinea, historical *in situ* dataset suffers from sparse sampling providing little information on the river plume variability (Da-Allada *et al.*, 2013). In addition, few model studies have focused on the Eastern Gulf of Guinea SSS dynamics (Camara *et al.*, 2015). SSS satellite missions offer a new opportunity, to investigate the eastern Gulf of Guinea river plume dynamics. Furthermore, the recent enhancement of database in the Gulf of Guinea (Argo, TSG and CTD casts) provides new perspective to investigate the stratification and small-scale vertical structure within the region's river plumes (Houndegnonto *et al.*, 2021).



Climate Change Initiative+ (CCI+)
Phase 1
Product Validation and
Intercomparison Report

Ref.: ESA-CCI-PRGM-EOPS-SW-17-0032

Date: 9/12/2021

Version : v3.0

Page: 35 of 59

A first step is to validate the CCI+SSS products in the Eastern Gulf of Guinea (GG). In the Gulf of Guinea (15°S-10°N/10°W-15°E), the available in situ SSS observations in the upper 5-10 m depth (TSG, Argo and CTD casts) have been co-located with CCI+SSSv2.31 products (Figure 10 ab). Scatter plots for TSG and Argo/CTD products reveal very good agreement with insignificant biases (~ 0.01 pss), and a RMSD of 0.46 pss for the comparison with TSG data and 0.36 pss for the comparison with the Argo and CTD data. These difference in RMSD can be explained by the larger spread of the in situ/CCI+SSSv2.31 products near the coast (Figure 10). Note that, the statistics in the GG are slightly worse (RMSD: ~ -0.02) than for the collocation of the SSS+CCIv1 reported in the previous PVIR report. TSG measurements are generally carried out closer to the coast where residual coastal biases and RFI contamination can increase the noise in the satellite measurement (Figure 10c).

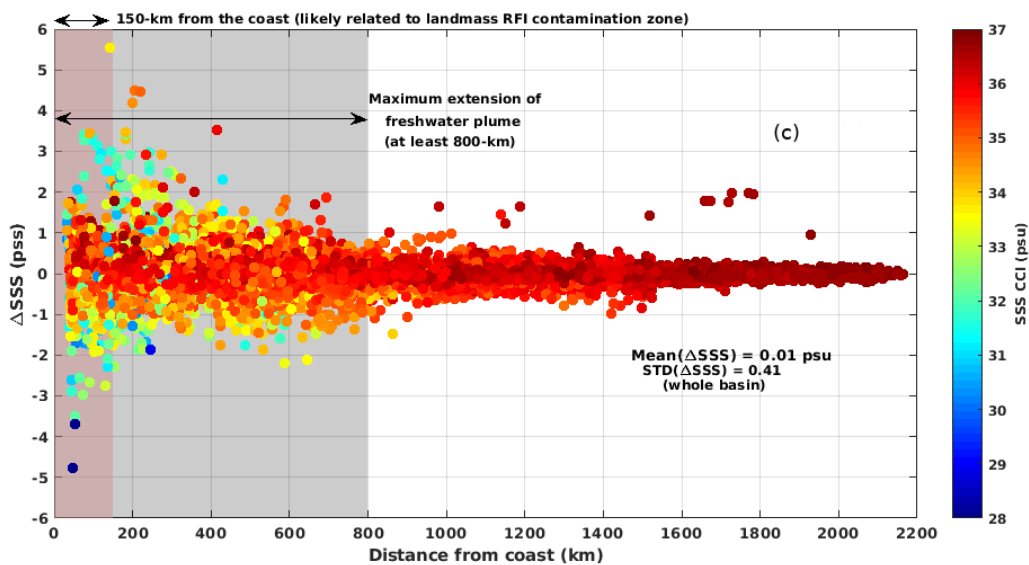
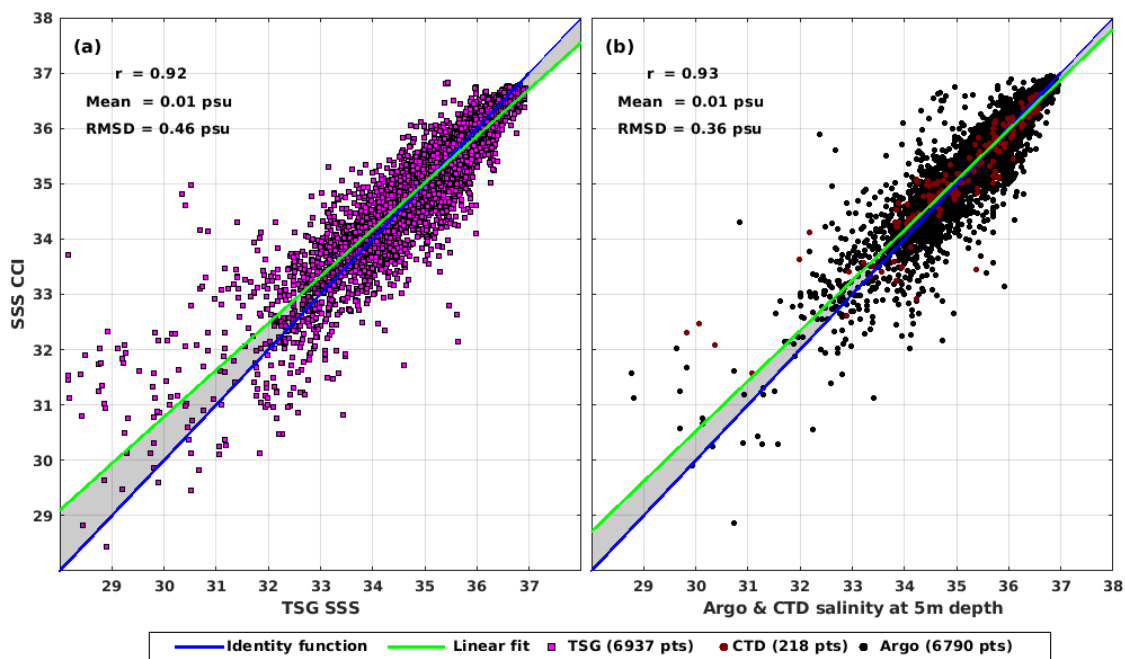


Figure 10: Scatter plot of TSG SSS measurements (a) and Argo/CTD data (b) with the CCI+SSS v2.31 products in the Gulf of Guinea (15°S-10°N/10°W-15°E) over the period 2010-2019. (c) distribution of the difference of co-located in situ/CCI+SSSv2 (in pss) as a function of the distance from the coast.



Climate Change Initiative+ (CCI+)
Phase 1
Product Validation and
Intercomparison Report

Ref.: ESA-CCI-PRGM-EOPS-SW-17-0032
Date: 9/12/2021
Version : v3.0
Page: 37 of 59

Moreover, near the coast the river plume signal generates, strong SSS horizontal gradients and shallow surface salinity stratification, thus it implies larger difference between *in situ* observation and satellite products.

References:

Boutin J, , J.L. Vergely, S. Marchand, F. D'Amico, A. Hasson, N. Kolodziejczyk, N. Reul, G. Reverdin and J. Vialard (2018): New SMOS Sea Surface Salinity with reduced systematic errors and improved variability. *Remote sensing of the Environment*, 214, 115-134. doi:10.1016/j.rse.2018.05.022.

Callies, J., and R. Ferrari, (2013), Interpreting energy and tracer spectra of upper-ocean turbulence in the submesoscale range (1–200 km), *J. Phys. Oceanogr.*, 43, 2456–2474, doi:10.1175/JPO-D-13-063.1.

Camara, I., N. Kolodziejczyk, J. Mignot, A. Lazar, and A. T. Gaye (2015), On the seasonal variations of salinity of the tropical Atlantic mixed layer, *J. Geophys. Res. Oceans*, 120, 4441–4462, doi:10.1002/2015JC010865.

Chelton, D. B., R. A. de Szoeke, and M. G. Schlax (1998), Geographical variability of the first Rossby baroclinic radius of deformation, *J. Phys. Oceanogr.*, 28, 433–460.

Da-Allada, C. Y., G. Alory, Y. du Penhoat, E. Kestenare, F. Durand, and N. M. Hounkonnou (2013), Seasonal mixed-layer salinity balance in the tropical Atlantic Ocean: Mean state and seasonal cycle, *J. Geophys. Res. Oceans*, 118, 332–345, doi:10.1029/2012JC008357.

Fox-Kemper, B., R. Ferrari, and R. Halberg (2008), Parametrization of the mixed layer eddies. Part I: Theory and diagnosis, *J. Phys. Oceanogr.*, 38(6), 1145–1165.

Houndegnonto, O.J., N. Kolodziejczyk, C. Maes, B. Bourlès, C. Da-Allada, and N. Reul (2021): Seasonal variability of freshwater plumes in the eastern Gulf of Guinea as inferred from satellite measurements. *Journal of Geophysical Research: Oceans*, 126, <https://doi.org/10.1029/2020JC017041>

Kilpatrick, K. A., G. Podestá, S. Walsh, E. Williams, V. Halliwell, M. Szczodrak, O. B. Brown, P. J. Minnett, and R. Evans (2015). A decade of sea surface temperature from MODIS. *Remote Sensing of Environment*, 165, 27-41. <http://dx.doi.org/10.1016/j.rse.2015.04.023>.

Kolodziejczyk, N., O. Hernandez, J. Boutin, and G. Reverdin (2015), SMOS salinity in the subtropical north Atlantic salinity maximum. Part II: Horizontal thermohaline variability, *J. Geophys. Res. Oceans*, 120, 972–987, doi:10.1002/2014JC010103.

Kolodziejczyk, N., G. Reverdin, J. Boutin, and O. Hernandez (2015), Observation of the surface horizontal thermohaline variability at mesoscale to submesoscale in the north-eastern subtropical Atlantic Ocean, *J. Geophys. Res. Oceans*, 120, doi:10.1002/2014JC010455.

Levy, M., and A. P. Martin (2013), The influence of mesoscale and submesoscale heterogeneity on oceanbiogeochemical reactions, *Global Biogeochem. Cycles*, 27, doi:10.1002/2012GB004518

Reul, N., B. Chapron, T. Lee, C. Donlon, J. Boutin, and G. Alory (2014), Sea Surface Salinity structure of the meandering Gulf Stream revealed by SMOS sensor, *Geophys. Res. Lett.*, 41, 3141–3148, doi:10.1002/2014GL059215.

4.2 Time series stability: intra-annual & long-term stability

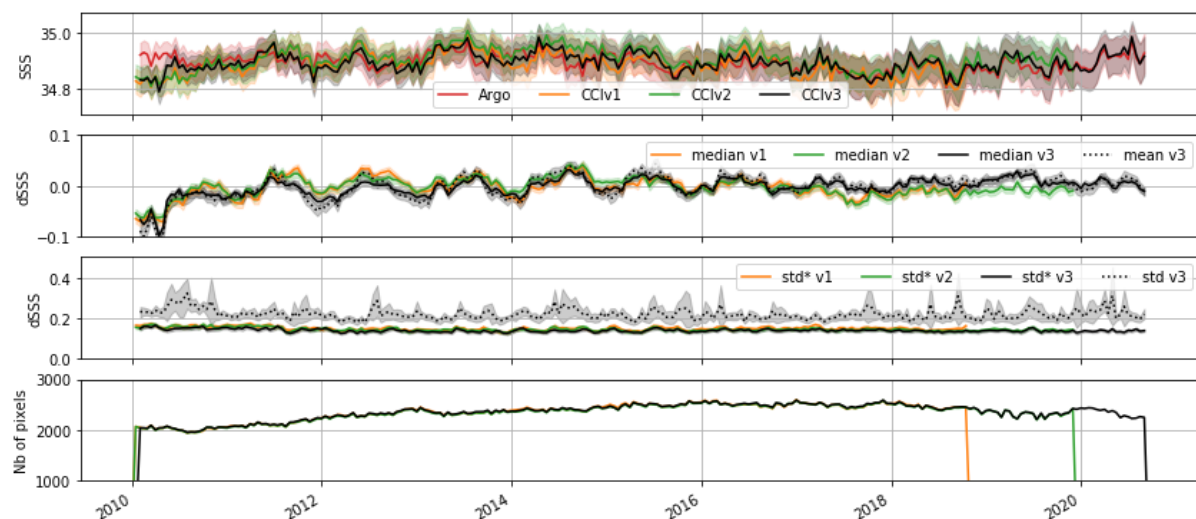


Figure 11: (1st panel): mean SSS of gridded MDB of pairwise Argo in red and L4 CCI measurements in orange, green and black for v1, v2 and v3; (2nd panel) Average of; (3rd panel) standard deviation of; the gridded MDB of the pairwise SSS difference between CCI and Argo. Solid lines represent (2nd panel) the median (3rd panel) the robust standard deviation. Dashed lines represent (2nd panel) the mean (3rd panel) the standard deviation. The shading indicates the 95% confidence interval. 4th panel) number of valid gridded MDB values.

The time series in Figure 11 represents the temporal evolution of gridded MDB of the pairwise measurements of CCI (L4 v1, v2, v3) and Argo and their differences. The mean SSS temporal variability represented on the top panel shows good agreement between CCI and Argo with a mean around 34.9 pss. The beginning of the period in 2010 highlights a lower value for CCI than Argo of less than 0.1 pss. The two middle panels represent the gridded MDB of the pairwise differences of CCI with Argo for average difference (mean and median); and dispersion (classic std and robust std). The global, temporal difference remains within ± 0.05 pss. There is a small but appreciable global seasonal cycle with a minimum at the beginning of each year. The amplitude decreases with time, in particularly since 2015. The dispersion, as estimated by the robust std of the difference, stays relatively constant over the full time series between 0.13 pss and 0.16 pss. However, the classic standard deviation presents some

peaks suggesting more extreme values in the tail of the distribution. Globally, the three CCI L4 versions are very similar. The number of valid pixels in the gridded MDB for each time step (bi-weekly) is indicated in the bottom panel. It slightly increases in time, directly link to the increase of the number of Argo profiles from 2010 to 2016.

The same L4v3 gridded MDB, as in Figure 11, are reproduced in Figure 12 to simplify comparisons with Level 3 data. From the top panel, representing the global mean SSS, the main feature is L3 SMOS has a higher variability than that observed by Argo and other CCI products (i.e. L4 and L3 for Aquarius and SMAP data). Differences between SMOS and L4 or Argo during the first six months in 2010 exceed 0.1 pss. This period corresponds to the SMOS commissioning phase which ends in May 2010. The second panel represents the median pairwise gridded difference between CCI products and Argo. The small trend in 2010, at the beginning of the time series, is similar for L4 and SMOS (median in this panel versus mean in the top panel as the latter average is more affected by outliers from RFI). The global seasonal cycle with a minimum at the beginning of each year is visible for L3 Aquarius, L4 and L3 SMOS data but its amplitude is stronger for the latter. With the inclusion of SMAP data in February 2015, the amplitude of L4 differences decrease. In this second period, SMOS oscillation amplitude is smaller than before 2015. SMAP oscillation is smaller than for SMOS, but they are in phase opposition, which perhaps explain why L4 is more stable in this second period.

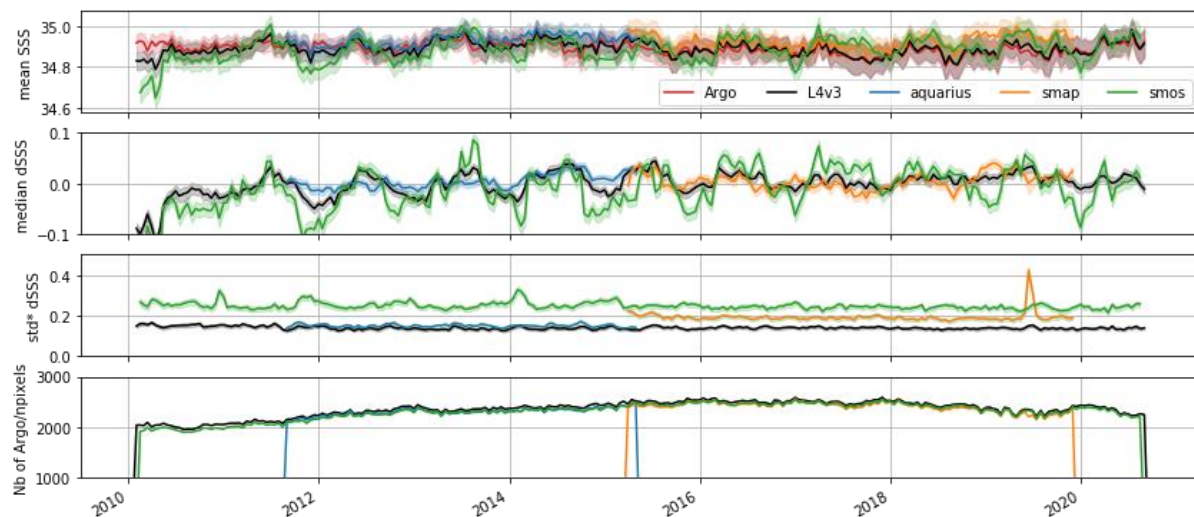


Figure 12 (1st panel): SSS mean of gridded MDB of the pairwise CCI and Argo measurement; (2nd panel) Median of; (3rd panel) robust standard deviation of; the gridded MDB of the pairwise SSS difference between CCI and Argo. (4th panel) number of valid gridded MDB values. The colours of the curves correspond to the data indicated in the legend.

Concerning the precision (robust std of the difference), L4 is constant over the full time series varying between 0.13 pss and 0.15 pss, even during the period with only SMOS data, and is better than any other product taken independently. For L3 products, the best precision against Argo is for Aquarius (0.14-0.16 pss), then for SMAP (0.18-0.20 pss) and SMOS (0.23-0.27 pss). The peak in std* of SMAP corresponds to the period during which SMAP was in safe



Climate Change Initiative+ (CCI+)
Phase 1
Product Validation and
Intercomparison Report

Ref.: ESA-CCI-PRGM-EOPS-SW-17-0032
Date: 9/12/2021
Version : v3.0
Page: 40 of 59

mode (19 June 2019 to 23 July 2019). For both SMOS and SMAP the std* is slightly higher at the beginning of their time series.

The temporal variability of the gridded MDB of the pairwise CCI/Argo differences is further assessed using latitude-time (Hovmöller) plots over the global ocean (Figure 13) for the L4 and L3 products. About half of the pixels are not significantly different from zero (at 95%). It appears there are significant oscillating signals with stronger amplitudes at higher latitude for all analysed CCI products (L4, L3C). The amplitude is of the same order of magnitude for L4, L3 Aquarius and L3 SMAP, but is stronger for L3 SMOS. For all cases, the oscillation is in phase opposition between Northern and Southern hemisphere. This means the CCI data are fresher in winter than Argo. The first 6 months in 2010, indicates CCI L4 and L3C SMOS are fresher than Argo particularly in the Northern hemisphere at high latitudes. A more quantitative estimate is provided in Figure 15. There is a small trend in L4 - and to a lesser extend for L3C Aquarius, SMAP and SMOS - from fresher (blue) to saltier for latitudes between 0°N and 30°N. A symmetric trend exists in the southern hemisphere.

The spatial representation of seasonal climatology of the gridded pairwise difference (Figure 14), calculated using the median for each season over the full time series, highlights fresher CCI L4 in the Northern hemisphere in Winter (DJF) but saltier in Summer (JJA). This is particularly clear around Japan and in the northern North-Atlantic, which are regions characterized by intermittent strong RFIs. A seasonal spatial signature is less pronounced and significant in the Southern hemisphere. Some local seasonal differences are visible close to the coast, generally related to river plumes, potentially associated with vertical stratification (see details in section 4.3). The seasonal average spatial patterns for L3 Aquarius and SMOS are very similar to L4, but with a higher amplitude for SMOS. SMAP has a low amplitude and different pattern, possibly reflecting the better RFI sorting from SMAP.

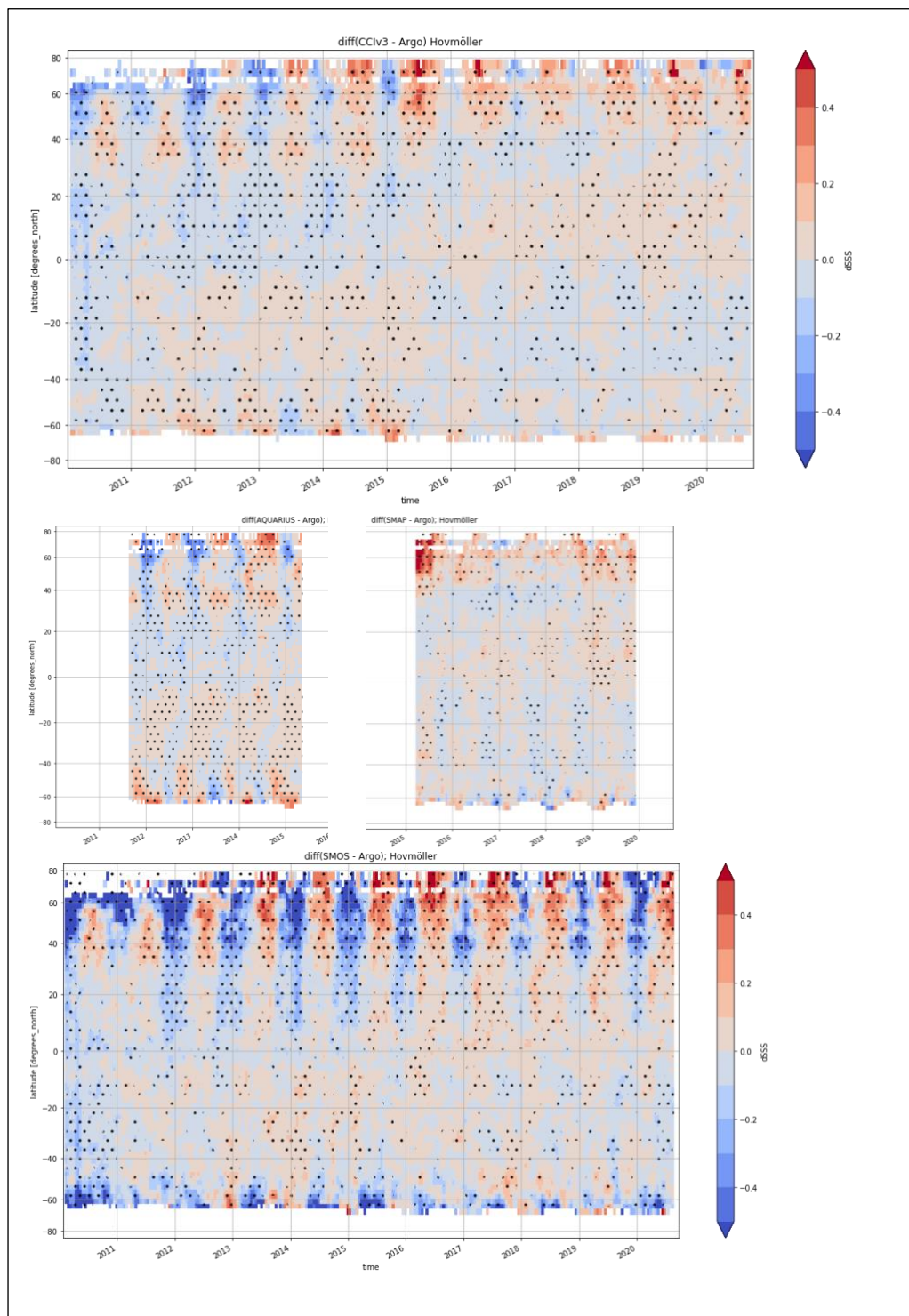


Figure 13: Global latitude-time Hovmöller of the gridded MDB of the pairwise CCI difference with Argo for (top) L4 v3; (middle-left) L3C Aquarius; (middle-right) L3C SMAP; (bottom) L3C SMOS. Each pixel represents the median value after a moving window over 2 pixels in latitude and time. Data which are significantly different from 0 (at 95%) are indicated with dots. All sub-figures share the same colour bar.

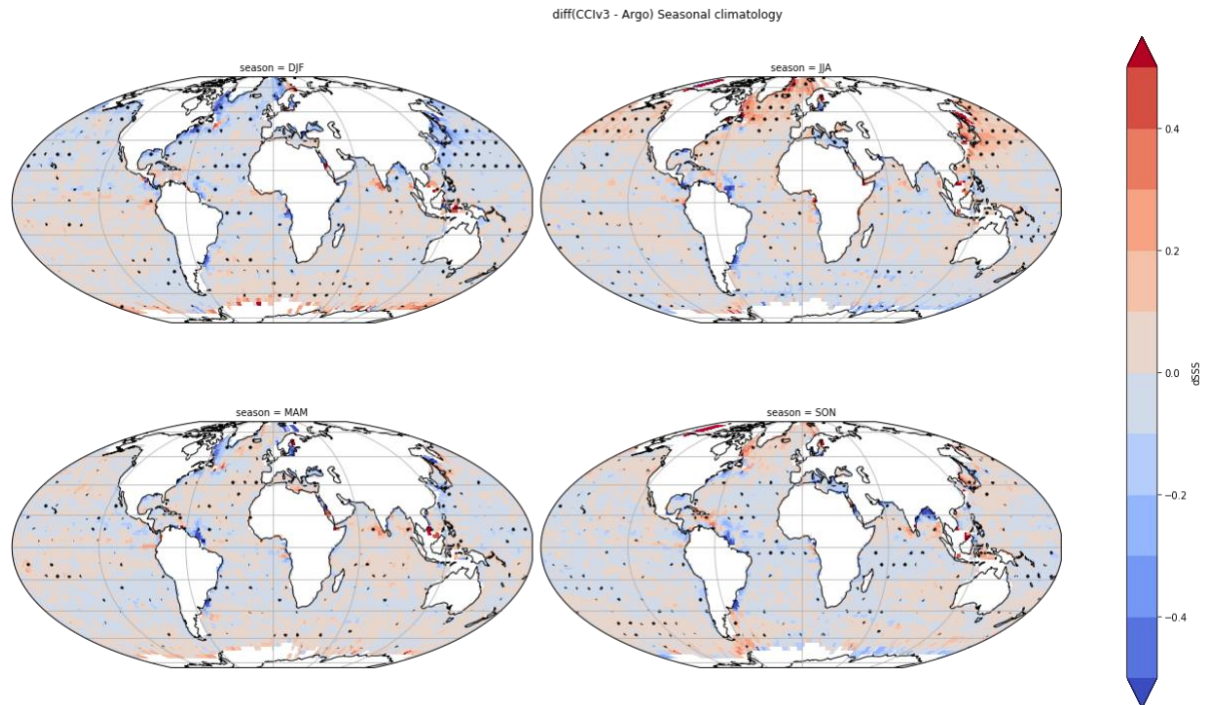


Figure 14: Seasonal climatology of the gridded pairwise CCI L4 difference with Argo calculated using the median. A moving window average of 2 x 2 pixels in longitude and latitude have been applied to increase the number of sampled, hence the significance. Pixels, which are statistically significant (at 95%) are indicated with dots.

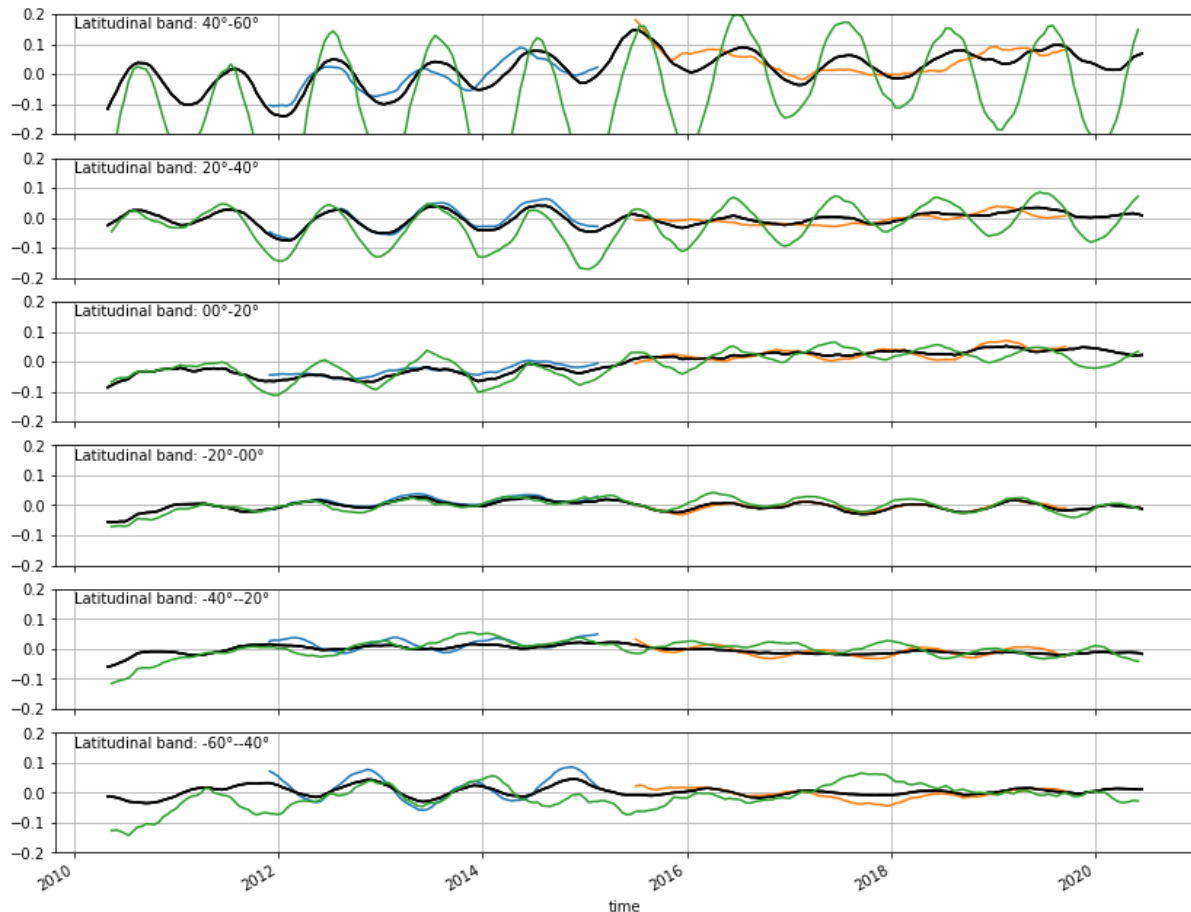


Figure 15: Latitudinal band (20° wide) median of the gridded pairwise SSS difference between CCI and Argo from (top) to (bottom) of [40°N;60°N] to [40°S;60°S]. A yearly rolling average is further applied to the data. Curves are in (black) for L4v2; (green) L3 SMOS; (blue) L3 Aquarius; (Orange) L3 SMAP.

Figure 15 represents 20° latitudinal median averages of the gridded pairwise MDB of the CCI (L4 and L3 Aq., SMAP and SMOS) / Argo differences with a yearly running average applied. The seasonal oscillation of the differences is strongly marked for the 40°N-60°N band (top panel). The seasonal cycle amplitude for this band is maximum for L3 SMOS with an amplitude generally exceeding 0.2 pss; for L4 and L3 Aquarius the amplitude is lower at about 0.1 pss. Variability in SMAP differences are above 0.1 pss but without a clear seasonal cycle at these latitudes. There is a positive trend of 0.2 pss in L4 and L3 Aquarius from 2010 to Autumn 2015 for 40°N-60°N.

Other latitudinal bands have smaller seasonal cycles in the difference. The other most significant band is the band 20°-40°N. The amplitude of the oscillation of 0.1 pss is similar for L4 and L3 SMOS and Aquarius data. Whereas the amplitude decreases with the inception of SMAP for L4, it only decreases in SMOS in 2017. For this band, SMAP and SMOS differences tend to be in phase opposition, although amplitude in SMAP oscillation is smaller.



Climate Change Initiative+ (CCI+)
Phase 1
Product Validation and
Intercomparison Report

Ref.: ESA-CCI-PRGM-EOPS-SW-17-0032
Date: 9/12/2021
Version : v3.0
Page: 44 of 59

Although the band 40°S-60°S presents a strong interannual variability there is no long-term seasonal cycle except during the Aquarius period for L4 and L3 Aquarius.

In terms of long-term stability, the following bands 60°S-40°S; 40°S-20°S; 20°S-0°; 10°S-10°N (not shown); 0°-20°N; 20°N-40°N are within ± 0.04 pss range for L4. Differences are similar for Aquarius and SMAP, but are larger for SMOS. All bands tend to have a positive trend for about the first 18 months of the time series. The variation in long term stability is maximum for the 40°N-60°N band as discussed above. Although very small, long term variations of the differences are opposite in sign between the 20°S-0° and 0°-20°N bands.

Applying latitude-time (Hovmöller) and latitudinal band averaging by ocean basin (Pacific, Atlantic, Indian) gives slightly different results (not shown). After excluding data in 2010, there is a good agreement between CCI L4 and Argo for both seasonal differences and long-term stability where the latter remains within ± 0.05 pss for Pacific and Atlantic Oceans between 40°S and 20°N and for Indian Ocean between 40°S and 10°S. Although differences between CCI and Argo are particularly strong in the Atlantic north of 40°N with consecutive minimum/maximum exceeding 0.3 pss before 2015, the amplitude decreases after 2015 staying just below 0.3 pss. In the Pacific, north of 40°N, the amplitude is below 0.3 pss up to end 2012 and decreases to 0.1 pss at the end of the time series. However, the oscillations are more pronounced in the Pacific ($> \pm 0.1$ pss) than in the Atlantic (generally ± 0.05 pss with peak at 0.1 pss) for the latitudinal band between 20°N and 40°N. In the Pacific for this band the amplitude of the difference decreases after 2015. Results by latitudinal band do not change when excluding data closer to 800 km to the coast.

4.3 In situ vertical representiveness error

The skin depth of satellite measurements depends on the wavelength; at a frequency of 1.4GHz, the skin depth is about 1cm. In most situation, this depth is expected to represent well the first meters of the upper ocean, but significant differences between the surface ocean and a few meters depth have been observed in fresh regions either for a few hours after a rainfall (typically 1 to 5 hours, depending on the wind conditions) (Boutin et al. (2016); Supply et al. 2020), or in river plumes where large differences can be found between the first meter and a few meters depth (e.g. Supply et al. 2020).

In order to get a global distribution of the vertical representiveness error, we calculate the gradient for each Argo profile between an acquisition depth of 5m and 10m. We use the same grid as for the pairwise comparison and take the median value of this gradient for each cell (in time and space). The seasonal climatology of this gradient in salinity is represented in Figure 16 highlighting that most of the ocean does not show a noticeable gradients between 5m and 10m, except in areas with strong freshwater fluxes (e.g. river plumes, ITCZ, Labrador current, ...). As expect, the surface at 5m is nearly always fresher than the based salinity at 10m. The surface is saltier only for very specific areas and periods as in the Mediterranean Sea in Summer but only with very small values. The strongest gradients in salinity relate to

the tropics for all seasons with typical values higher than 0.02 pss/m. If we extrapolate linearly the gradient from 5m to the surface, we might suspect differences due to the vertical sampling exceeding 0.1 pss. In Summer, vertical gradients appear in the Northern Hemisphere in the vicinity of the western boundary current (Gulf Stream and Kuroshio).

These results suggest the SSS measured by satellite would tend to be fresher than the one measured in situ by Argo. However, this effect is an order of magnitude less than the seasonal one observed on Figure 14 so that the mean difference CCI minus Argo on Figure 14 does not reflect the patterns below.

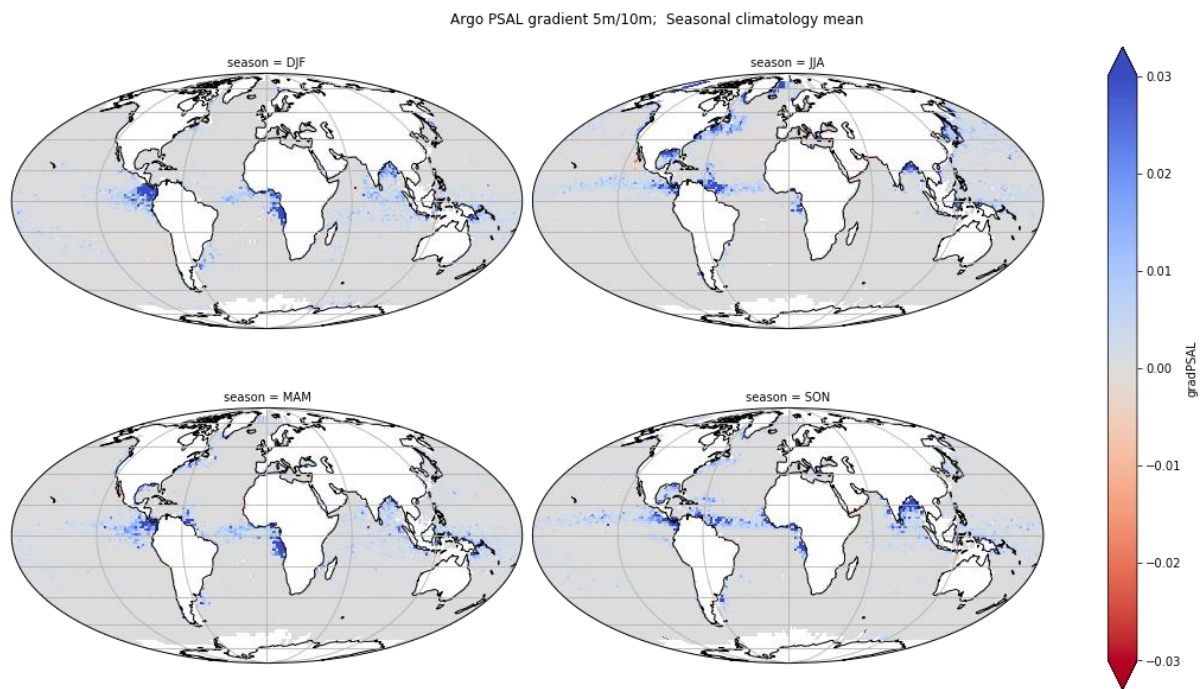


Figure 16: Seasonal Salinity gradient (in pss/m) derived from Argo between 5m and 10m. Gradient are gridded on the same grid as used for the pairwise difference (bi-weekly; 175 km).

4.4 Temporal & spatial effective resolution

4.4.1 SSS temporal variability at different time scale (Case Study 5: J. Köhler, M. Sena-Martins, D. Stammer)

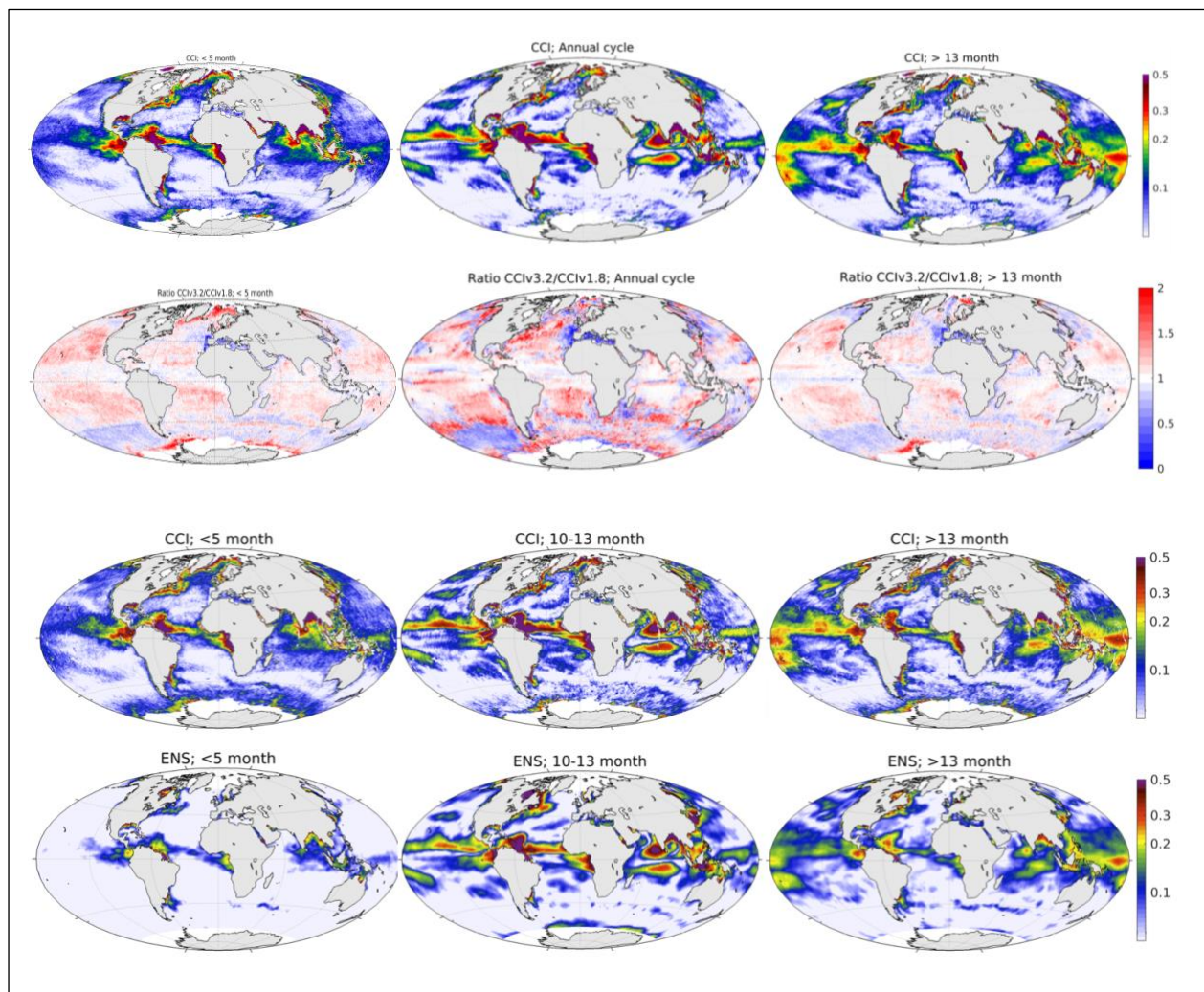


Figure 17: STD of (left) high-pass (<5 months) filtered time series; (middle) annual cycle; (right) low-passed (>13 months) filtered time series of (1st row) CCI+SSS L4v3 data; (2nd row) ratio between 1st and 3rd row or equivalently between v3 and v1; (3rd row) CCI+SSS L4v1 data; (bottom row) ensemble in situ data. All data used the same time period up to 2018.

An assessment of the high-frequency SSS variability is published in (Stammer et al., 2020). Figure 17 compares an ensemble of in situ observations (details in the publication) with the respective CCI L4 product for different time scale. It shows that the higher temporal resolution of the satellite data leads to more meaningful small-scale high-frequency variability than in situ data. The magnitude of variability is approximately 1.5 times higher for CCI+SSS L4v1 than for the ensemble in situ salinity, and larger differences between the



Climate Change Initiative+ (CCI+)
Phase 1
Product Validation and
Intercomparison Report

Ref.: ESA-CCI-PRGM-EOPS-SW-17-0032

Date: 9/12/2021

Version : v3.0

Page: 47 of 59

spatial patterns are observable in the Gulf Stream region, Amazon outflow, eastern tropical Pacific, north-eastern Indian Ocean and around the maritime continent.

The annual cycle presents large amplitude in the ITCZ region, again off the major rivers and frontal regions. Here, the satellite and in situ fields show corresponding patterns, varying only slightly in magnitude. Larger differences between CCI v1 and in situ variability spatial patterns and magnitudes can be observed in their low-frequency variability, in that interannual variability patterns are much larger for CCI+SSS than for the in situ data, especially in the central Indian Ocean, the major river outflow regions and the Northern North Atlantic. Higher amplitudes are also present in the equatorial Pacific Ocean in regions of strong vertical stratification, where the top surface variability is better sampled by satellite than in situ, as detailed in section 4.3. On the other hand, many of the patterns have direct relationships to physical mechanisms such as run-off from large rivers.

CCI v3 shows more variability in the mid latitudes compared with v1 and less variability near coastal regions where RFI is present. CCIv3 is slightly less variable at low frequency than v1 and closer to the in situ data variability.

4.4.2 Temporal resolution

The average temporal power spectra of SSS from all moorings and CCI collocations from the PiMEP MDB are represented in Figure 18 for the weekly products and in Figure 19 for the monthly products. ISAS optimal interpolation SSS and the SSS from the Mercator numerical circulation model are also shown. CCI L4 and L3 products shows as expected a decrease at the Nyquist frequency (respectively 14 days and 60 days). For the weekly products, whereas the merged L4 products power spectrum is very low for frequency higher than a week, they stay relatively high, with rebound, for the individual satellite products (Aquarius, SMAP or SMOS). The fact that the L4 merged product does not reflect these higher frequency signals suggests that the individual signals from L3 are not coherent and might be due to acquisition artefacts.

CCI L4 and CCI L3 Aquarius power spectra are well aligned with the one for the moorings, but this is not the case for CCI L3 SMAP and SMOS products which might be explained by stronger noise floor of these satellites. On contrary, for the monthly products, all L4 and L3 products are well aligned with the one from the moorings.



Climate Change Initiative+ (CCI+)
Phase 1
Product Validation and
Intercomparison Report

Ref.: ESA-CCI-PRGM-EOPS-SW-17-0032
 Date: 9/12/2021
 Version : v3.0
 Page: 48 of 59

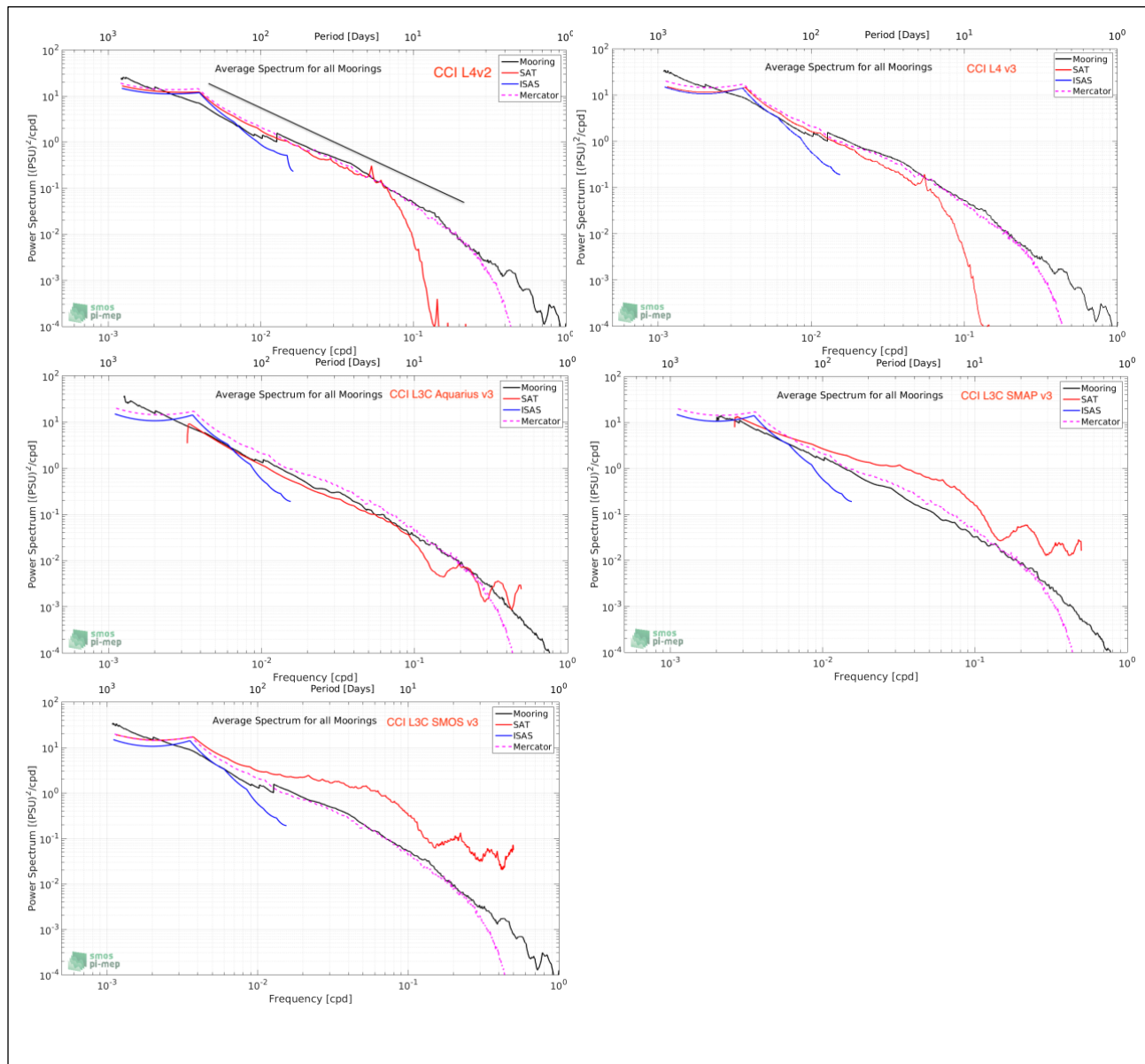


Figure 18 : Average power spectrum of SSS from (black) moorings, (red) CCI weekly products stated in legend, (blue) ISAS, (pink) Mercator; from PiMEP.

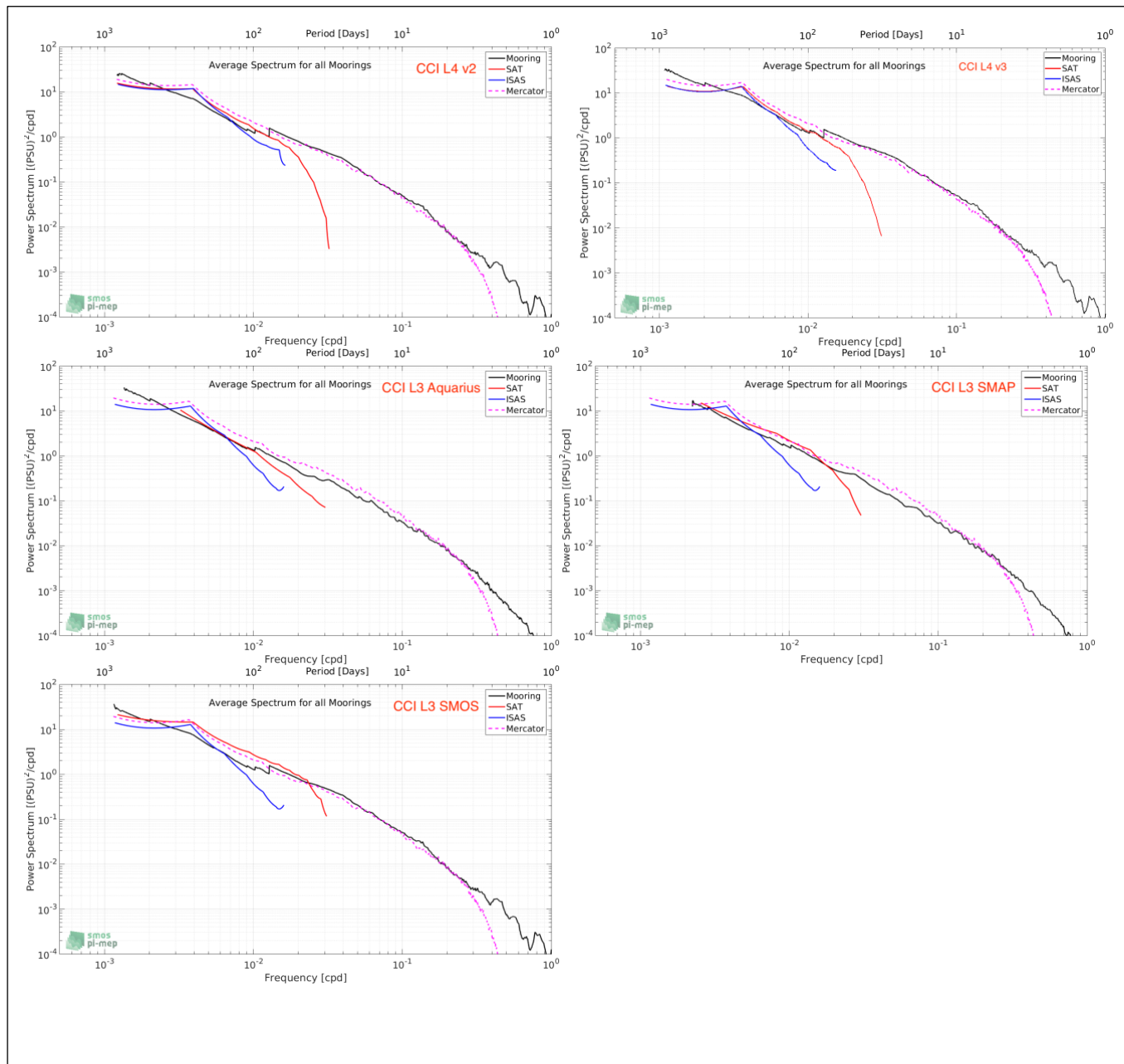


Figure 19: same as above but for the Monthly products.

4.4.3 Assessment of mesoscale features in Tropical Atlantic (Case Study 4: N. Kolodziejczyk, N. Reul)

The surface mixed layer thermohaline structures at meso-scale to submesoscale (smaller than the local radius of deformation, *Chelton et al., 1998*) are ubiquitous features in the global



Climate Change Initiative+ (CCI+)
Phase 1
Product Validation and
Intercomparison Report

Ref.: ESA-CCI-PRGM-EOPS-SW-17-0032

Date: 9/12/2021

Version : v3.0

Page: 50 of 59

ocean. They contribute to horizontal and vertical heat and salt exchange and vertical re-stratification (Fox-Kemper *et al.*, 2005). They have a global impact on ocean circulation and climate since they contribute to the cascade of energy from large scale toward the smallest scales of diffusive mixing (Callies and Ferrari, 2013). Eventually, they have a major impact on bio-geochemistry and ecosystems. The submesoscale processes are characterized by very intense vertical velocities that allow strong exchanges of carbon, oxygen and nutrient between the surface and subsurface ocean (Lévy and Martin, 2013).

Until early 2010, satellite capabilities for observing surface thermohaline variability have mainly relied only on the observation of Sea Surface Temperature (SST), resolving small scale features such as 10 km (Kilpatrick *et al.*, 2015). In contrast, synoptic image of Sea Surface Salinity (SSS) were not available and *in situ* SSS at high resolution are only available from a few high resolution sections from Thermosalinograph (TSG) surveys from ships of opportunity, repeated transects or cruise campaign (Kolodziejczyk *et al.*, 2015b). Since 2010, thanks to ESA SMOS mission, then NASA Aquarius and SMAP missions, 4-7 days global maps of SSS at resolution between 40-100 km are now available permitting observation of larger mesoscale features in subtropical and tropical region (Reul *et al.*, 2014; Kolodziejczyk *et al.*, 2015a).

In order to verify the effective capability of the new CCI-SSS products v2.31 and v3.2 (7 days) to monitor the large mesoscale features of SSS in the subtropical and tropical regions, the CCI SSS were systematically co-localized and compared with TSG SSS along existing repeated transects in the Subtropical North Atlantic and Tropical Atlantic. A effective metric to assess the SSS horizontal variance and scale content of both products is to compute the spectra and coherency spectra between TSG SSS and CCI-SSSv2.31 and v3.2 (Boutin *et al.*, 2018).

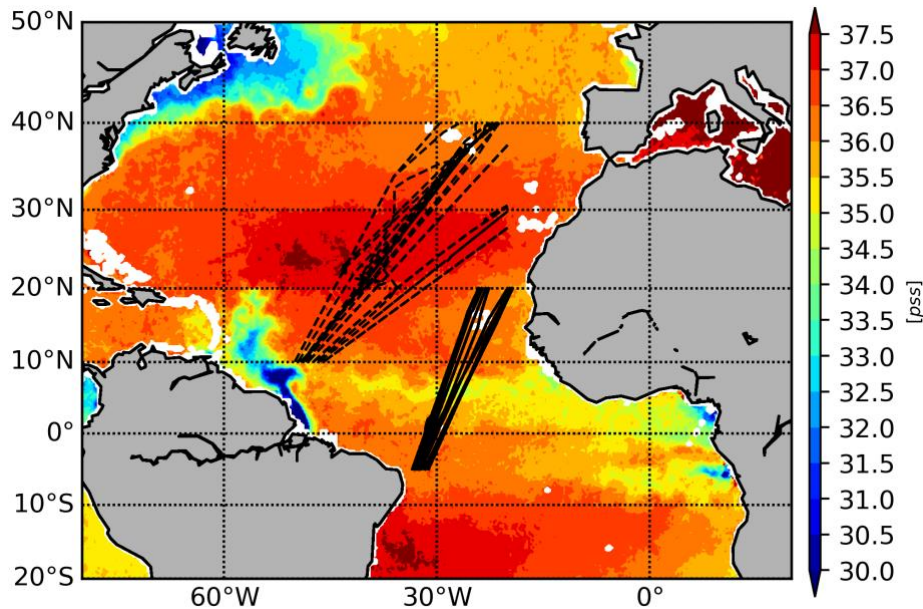


Figure 20: CCI+SSS on 30 June 2011 with 93 TSG transects in the Subtropical North Atlantic (dashed) and 26 TSG transect in the Tropical Atlantic.

SSS TSG transects were collected from ships of opportunity (representative of salinity at 10 m depth), resolving horizontal SSS features at around 2-3 km (Alory *et al.*, 2015). Two regions were chosen for the present study (Figure 20): i) the North Atlantic subtropical SSS maximum (50-20°W/10-40°N), where 88 transects between 2011-2016 are available; and ii) the Tropical Atlantic (40-10°W/5°S-20°N) where 26 transects between 2014-2016 are available. Individual transects were visually inspected and suspicious transects were discarded. In order to reduce uncertainty due to noisy individual spectrum from each individual transect, spectra were averaged for both regions.

The horizontal SSS coherency spectra refers to the coherency of the SSS horizontal variability between the co-located TSG SSS and CCI+SSS products, *i.e.* the level of correlation of the SSS signal for a given wavelength range. This allows the assessment of the actual capability of CCI+SSS products to observe mesoscale features (>50 km) from the noise and spurious SSS contamination.

In the Subtropical North Atlantic (Figure 21a), in spite of slightly less energy between 50-1000 km wavelength, CCI+SSSv2.31 and v3.2 horizontal variance spectrum for both TSG and CCI+SSS spectra show good agreement, *i.e.* comparable slopes between 50-1000 km are observed. This suggests that for this range of wavelength the variance of mesoscale features is probably smoothed in CCI+SSS products. However, the CCI+SSSv2.31 spectrum exhibits slightly more energy than the CCI+SSSv3.2 spectra. Interestingly, the coherency spectra (Fig.2b) exhibits a quasi-linear decrease from large scale (coherency>0.75 for wavelength >



Climate Change Initiative+ (CCI+)
Phase 1
**Product Validation and
Intercomparison Report**

Ref.: ESA-CCI-PRGM-EOPS-SW-17-0032

Date: 9/12/2021

Version : v3.0

Page: 52 of 59

1000 km) to mesoscale (coherency \sim 0.30 for wavelength \sim 300 km). The significance at 95% is lost for wavelength below 200 km. This suggests that wavelengths smaller than 300 km are poorly represented in the CCI+SSS product. The CCI+SSSv2.31 spectrum exhibits slightly less coherency than the CCI+SSSv3.2 spectrum, this is likely due to slightly noisier SSS v2.31 fields. Overall, these results are consistent with a previous study on investigating the SMOS LOCEAN CEC L3 product (*Boutin et al.*, 2018) in the same region, however, with a slightly improved coherency for CCI+SSS product. As such, no significant differences from the previous PVIR-CCI+SSS report are reported.

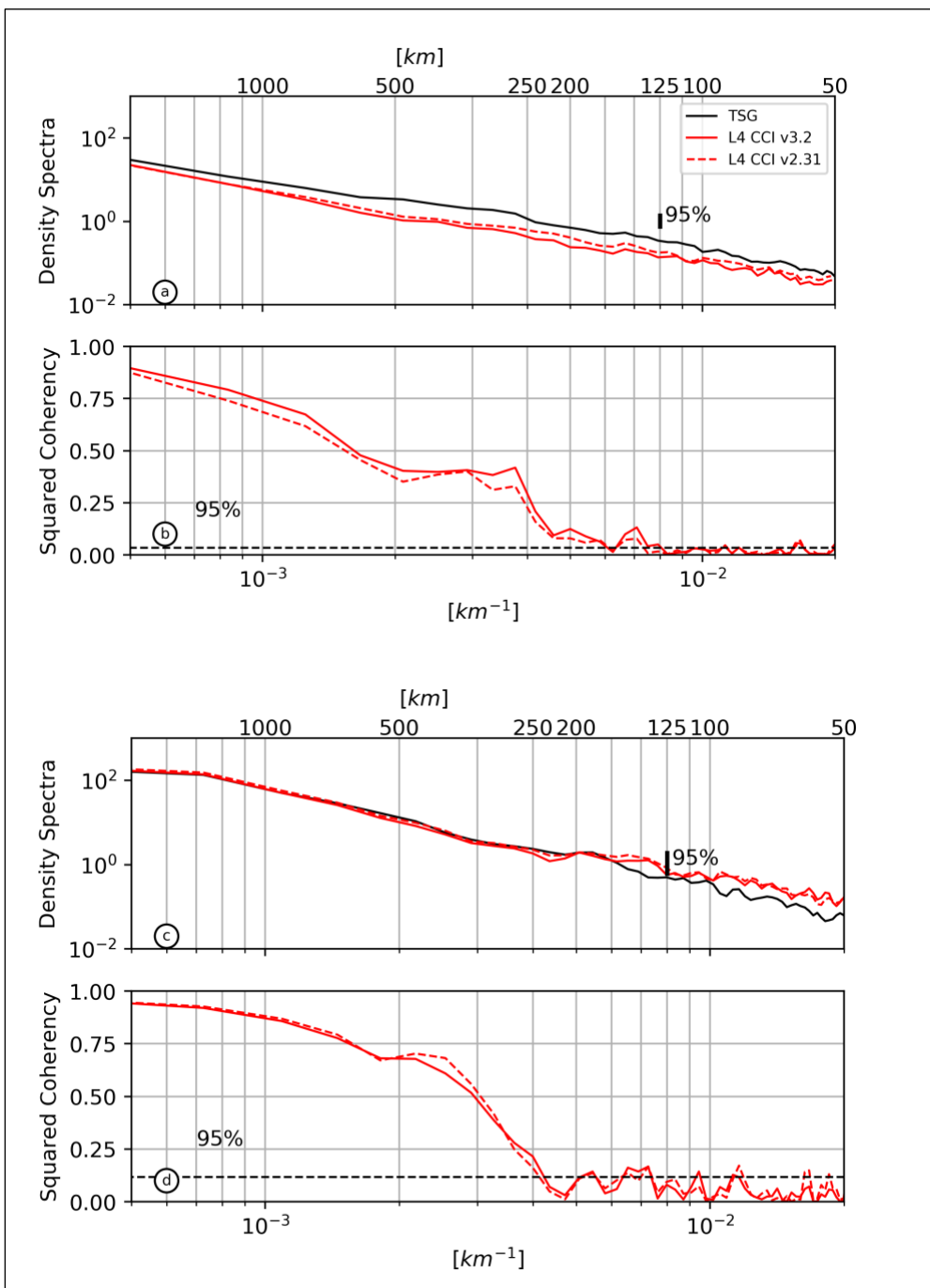


Figure 21: a) Density spectra from from 88 collocated TSG (black); CCI+SSS v2.31 (dashed red); CCI+SSS v3.1 (solid red) SSS transects in Subtropical North Atlantic. Vertical thick black bar is the level of confidence at 95%. b) Coherency between the TSG and CCI+SSS SSS transects. Dashed line is the level of significance at 95%. c) Density spectra from from 26 collocated TSG (black)/CCI+SSS(red) SSS transects in Tropical Atlantic. Vertical thick black bar is the level of confidence at 95%. d) Coherency between the TSG and CCI +SSS SSS transects. Dashed line is the level of significance at 95%.



In the Tropical Atlantic (Figure 21c), TSG and CCI+SSS spectra show very comparable behaviors in that, the level of variance and slope have comparable values. Furthermore, both spectra also show a relatively high level of coherence (Figure 21d) at wavelengths larger than 300 km (coherency>0.5). In the Tropical Atlantic region, the coherency drops off observed at wavelengths smaller than 250 km suggests that the CCI+SSS product is not able to consistently resolve scale smaller than 125 km. This is a slight improvement over the CCI+SSS v1 products reported in the previous PVIR report. No significant differences are reported between CCI+SSS v3.2 and v2.31.

In conclusion, in the subtropical Atlantic, the CCI+SSSv2.31 and v3.2 products are able to resolve wavelengths of the order of 300 km. This wavelength corresponds to horizontal mesoscale features of the order of about 150 km (gradient, eddy). However, the level of coherency between TSG SSS horizontal variability and CCI+SSS drops rapidly at the mesoscale. In the tropics, the level of coherency remains high up to 300 km wavelengths, then drops dramatically.

The loss of coherency at smaller horizontal wavelengths could be explained by i) the limiting resolution of SSS satellite mission (>50 km), ii) remaining noise and artifacts in the CCI+SSS data, and iii) smoothing from the objective analysis procedure of the CCI+SSS products. Nevertheless, it is worth pointing out that inconsistency between instantaneous and point-wise measurements from the TSG data and co-localized CCI+SSS products (7 days, 25 km) may be responsible for a shift and lag between TSG SSS measurements and CCI+SSS products resulting in loss of coherency for the smaller and faster SSS mesoscale structures.

4.5 Uncertainty

As explained in section 3.2 above, we will follow two approaches to validate satellite uncertainty estimates:

- Normalise the dSSS by the uncertainty with a centred reduced variable and analyse the variation compared to a theoretical behavior of a random normalised variable with mean of zero and std of one.
- Compare the dSSS distribution with the uncertainty estimates.

For both cases, we will consider the satellite uncertainty $\Delta\sigma_{sat}$ alone or the total uncertainty which combines the satellite uncertainty with the reference uncertainty itself which includes

the horizontal representiveness error ($\sigma_{tot} = \sqrt{\Delta\sigma_{sat}^2 + \Delta\sigma_{ref}^2}$).

4.5.1 Normalised SSS

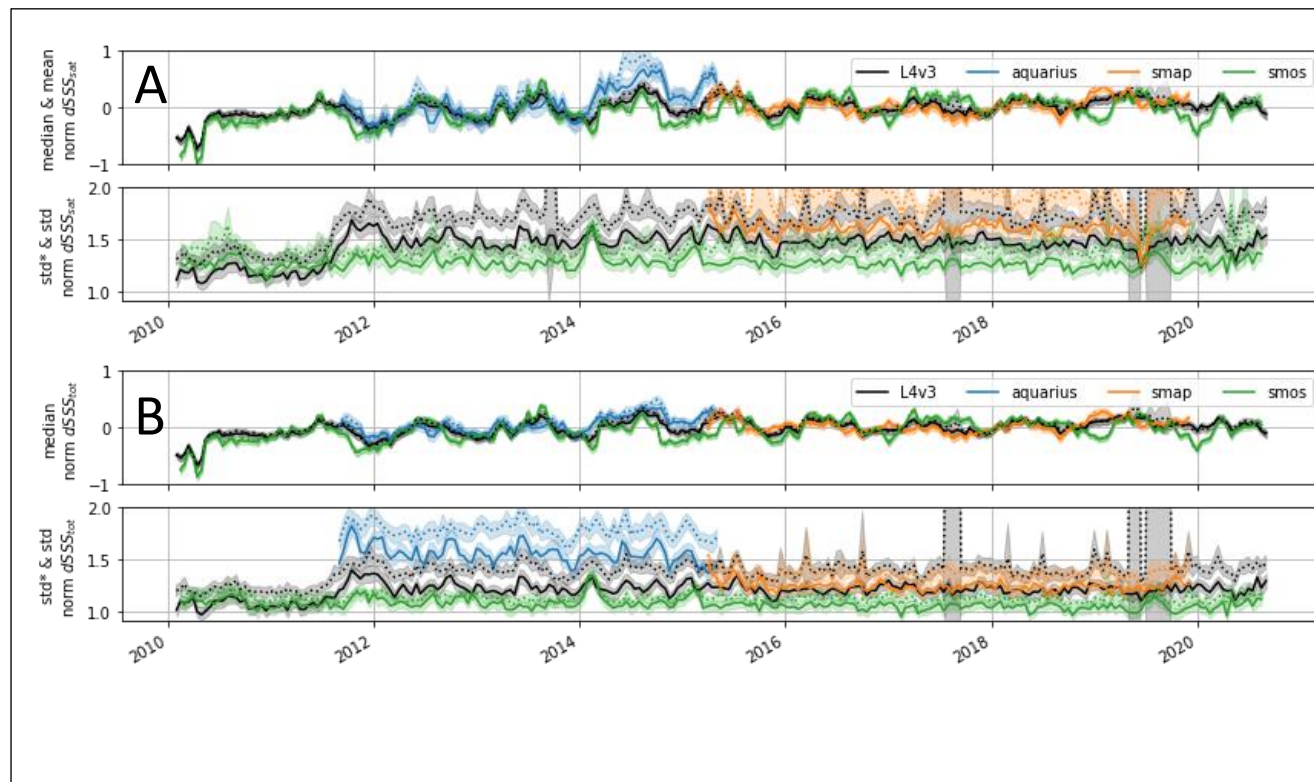


Figure 22 : Time series of the normalised SSS normalised using (A) the satellite uncertainty; (B) the total uncertainty combining the sat and reference uncertainty. (1st row for each panels) represent (solid line) the median and (dashed line) the mean. (last row for each panels) represent (solid line) the robust std and (dashed line) the classic std. (colours) are for the L4v3 and L3C Aquarius, SMAP and SMOS data.

Figure 22 represents a time series of the normalised dSSS using in (A) the provided satellite uncertainties and in (B) the quadratic mean of the provided satellite uncertainties plus the reference uncertainties described in the methods. The normalised SSS represented in (Figure 22A bottom rows) shows a standard deviation between 1 and 2 (excepted for L3C Aquarius between 2 and 4) when the normalisation uses only the provided satellite uncertainties. The robust std always gives slightly lower estimates than the classic std linked to remaining longer tail in the distribution. For a perfect estimation of the uncertainties we expect a std of 1. The higher values observed here are linked to the reference uncertainties linked to differences between pointwise measurements and pixel-averaged measurements. This is particularly strong for Aquarius with a resolution of ~100km. With the total uncertainties, including the reference representativeness error, std get closer to unity.

In detail, L3 SMOS is the closest to the unity and is rather constant in time. L4v3 “jumps” with the inclusion of Aquarius data and stays relatively constant in time for the rest of the period. L3 SMAP has similar values as L4v3. L3 Aquarius is still significantly higher than all other data despite the addition of the reference representativeness error.

The average (median, mean) time series of the normalised SSS (Figure 22 A/B 1st row) does not provide information about the uncertainty. For each point, we have about more than about 2000 observations (cf Figure 11 last row), leading to a theoretical variability (std) of the normalised SSS of 0.02 which is much higher than what we observe.

4.5.2 Compared SSS distribution

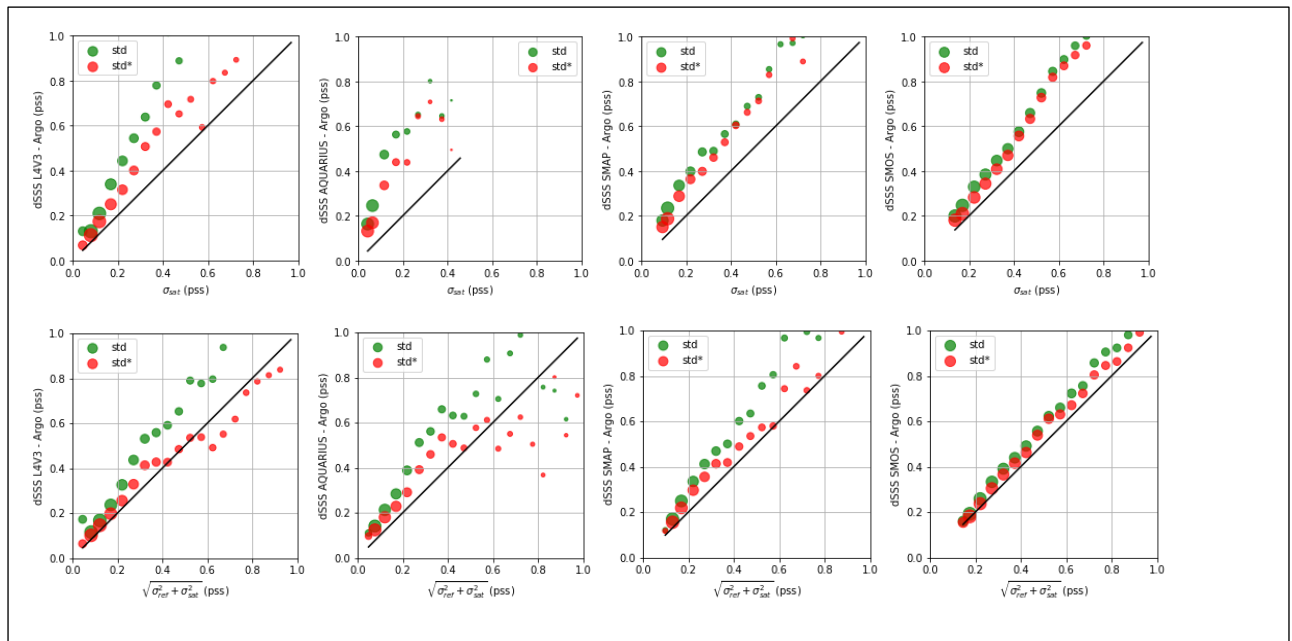


Figure 23: measured standard deviation (green and red dots) for resp. classic and robust std; of the gridded pairwise CCI/Argo difference for each uncertainty bins. (top) using satellite uncertainty; (bottom) using total uncertainty - sat + ref. (column from left to right) for L4v3, L3 Aquarius, SMAP, SMOS. The size of the circle indicates the number of data.

The gridded MDB of the pairwise differences are now binned by uncertainty bins of 0.05 pss wide (Figure 23) and computed over the full time series for each product. Columns correspond to respectively L4v3, Aquarius, SMAP and SMOS. The 1st row is using the provided satellite uncertainties, whereas the 2nd row is for the total uncertainties. Ideally the std (classic or robust) or the dSSS should follow a one-to-one relation. If one only takes into account the satellite uncertainties (1st row), then the observed std exceeds the satellite uncertainties but follows a nearly linear relation. On the contrary, if one adds the representativeness error, all products go closer to the one-to-one relation. SMOS has the best uncertainty estimate between 0 and 20%. L4v3 follows with values within +/-30% except for the first bin (total uncertainty between 0 and 0.05 pss) where observed dispersion is 40% higher. SMAP uncertainties tend to be underestimated (between 20%-40%) where total uncertainties are below 0.3 pss, but tend to be within 0-20% for higher total uncertainties. Aquarius total uncertainties are strongly underestimated between 30-60% below 0.4 pss, and particularly for uncertainties below 0.15 pss.



Climate Change Initiative+ (CCI+)
Phase 1
**Product Validation and
Intercomparison Report**

Ref.: ESA-CCI-PRGM-EOPS-SW-17-0032

Date: 9/12/2021

Version : v3.0

Page: 57 of 59

Page Intentionally Blank



Climate Change Initiative+ (CCI+)
Phase 1
**Product Validation and
Intercomparison Report**

Ref.: ESA-CCI-PRGM-EOPS-SW-17-0032

Date: 9/12/2021

Version : v3.0

Page: 59 of 59